

Title	Assessment of respiratory motor units in the mdx mouse model of Duchenne muscular dystrophy
Authors	Murphy, Kevin H.
Publication date	2021-03-22
Original Citation	Murphy, K. H. 2021. Assessment of respiratory motor units in the mdx mouse model of Duchenne muscular dystrophy. MRes Thesis, University College Cork.
Type of publication	Masters thesis (Research)
Rights	© 2021, Kevin H. Murphy. - https://creativecommons.org/licenses/by-nc-nd/4.0/
Download date	2023-05-05 13:41:19
Item downloaded from	http://hdl.handle.net/10468/11284



UCC

Coláiste na hOllscoile Corcaigh, Éire
University College Cork, Ireland

Assessment of Respiratory Motor Units in the *mdx* Mouse Model of Duchenne Muscular Dystrophy

Kevin H. Murphy, BSc (Hons)
Department of Physiology
University College Cork

*Thesis submitted to University College Cork for the award of **Master of Science***

Under the Supervision of:

Professor Ken D. O'Halloran
Head of Department and Chair
&
Dr. David P. Burns

Table of Contents	1
1 Chapter 1 – Introduction	5
1.1 Skeletal Muscle	6
1.1.1 Muscle Fibre Types	7
1.1.2 Respiratory Muscle	7
1.1.3 Diaphragm	8
1.1.4 Intercostal muscles	8
1.1.5 Genioglossus	9
1.1.6 Sternohyoid	9
1.2 Motor Units	10
1.2.1 Henneman's Size Principle	10
1.2.2 Rate Coding & Recruitment	11
1.3 Control of Breathing	11
1.3.1 Neural Control of Breathing	12
1.4 Respiratory Plasticity	13
1.4.1 Central Drive Plasticity	14
1.4.2 Phrenic motor neuron plasticity	14
1.4.3 Neuromuscular junction plasticity	15
1.4.4 Plasticity - Shifting the demands of respiratory motor pools	15
1.5 Dystrophin	16
1.5.1 Dystrophinopathies	16
1.5.2 Duchenne Muscular Dystrophy (DMD)	17
1.5.3 Pathophysiology of DMD	17
1.5.4 Sleep-disordered Breathing in DMD	18
1.6 Models of Duchene Muscular Dystrophy	19
1.6.1 Dystrophin deficient <i>mdx</i> mouse	19
1.7 Management of DMD	21
1.7.1 Corticosteroids	21
1.7.2 Utrophin	21
1.7.3 Exon Skipping	22
1.8 Aims and Hypothesis	22
2 Chapter 2 - Methods	24
2.1 Ethical approval	25
2.2 Experimental animals	25
2.3 Respiratory flow recordings in conscious wild-type and <i>mdx</i> mice	25
2.3.1 Whole-body plethysmography	25
2.3.2 Experimental Protocol	25
2.3.3 Data Analysis	26

2.4	Respiratory EMG and motor unit recordings in anaesthetised mice	26
2.4.1	Surgical preparation	26
2.4.2	Experimental Protocol	26
2.4.3	Intramuscular electromyography recordings	27
2.4.4	Motor unit spike sorting	27
2.4.4.1	Filtering	28
2.4.4.2	Detection	28
2.4.4.3	Feature Extraction	28
2.4.4.4	Clustering analysis	28
2.4.4.5	Data Analysis	28
2.5	<i>Ex vivo</i> diaphragm muscle function	31
2.5.1	Experimental Protocol	32
2.5.2	Data Analysis	33
2.6	Statistical Analysis	33
3	Chapter 3 – Results	35
3.1	Baseline ventilation and ventilatory responsiveness to hypercapnic-hypoxia in conscious mice	36
3.2	Respiratory muscle motor unit properties	38
3.2.1	Diaphragm	39
3.2.2	External Intercostals	40
3.2.3	Genioglossus	41
3.3	Respiratory muscle EMG activity in anaesthetised mice during baseline and chemostimulation	41
3.4	Diaphragm muscle contractile function <i>ex vivo</i>	45
4	Chapter 4 – Discussion	48
5	References	57
6	Publications	68
7	Conference Proceedings	68

List of figures

Chapter 2.

Figure 2.1. Intramuscular EMG recording and spike sorting process.	29
--	----

Chapter 3.

Figure 3.1. Respiratory flow traces.	36
Figure 3.2. Genioglossus (GG) motor unit properties in an anaesthetised wild-type mouse.	38
Figure 3.3. Diaphragm EMG and motor unit properties for anaesthetised mice during baseline conditions.	39
Figure 3.4. External intercostal EMG and motor unit properties for anaesthetised mice during baseline conditions.	40
Figure 3.5. Genioglossus EMG and motor unit properties for anaesthetised mice during baseline conditions.	41
Figure 3.6. Diaphragm, intercostal and genioglossus electromyogram (EMG) activity in anaesthetised mice.	42
Figure 3.7. Diaphragm electromyogram activity in anaesthetised mice during baseline and hypercapnic-hypoxia.	44
Figure 3.8. External intercostal electromyogram activity in anaesthetised mice during baseline and hypercapnic-hypoxia.	44
Figure 3.9 Genioglossus electromyogram activity in anaesthetised mice during baseline and hypercapnic-hypoxia.	44
Figure 3.10. Ex vivo diaphragm muscle contractions.	45
Figure 3.11. Ex vivo diaphragm muscle contractile force.	47

List of tables

Chapter 2.

Table 2.1. Detection functions, parameters, definition and set values considered for forming and holding motor unit templates.	31
--	----

Chapter 3.

Table 3.1. Breathing during normoxia and hypercapnic-hypoxia	37
Table 3.2. Ex vivo respiratory muscle contractile kinetics.	46

Chapter 1: Introduction

1. Introduction

1.1 Skeletal Muscle

Skeletal muscle makes up approximately 40% of total body mass making it the most abundant tissue in the human body (Gransee *et al.*, 2012). Skeletal muscle tissue comprises numerous multi-nucleated muscle cells, collectively known as muscle fibres, which work in a unitary fashion to support contraction. The endomysium, a protective layer made up of connective tissue, surrounds muscle fibres. Fibre bundles, known as fascicles, are covered with a connective tissue layer known as the perimysium. The epimysium coats bundles of fascicles (muscle) with a connective sheath (Lieber, 2002). Skeletal muscles have a striated appearance due to the highly organised arrangement of thick and thin filaments within myofibrils and due to the alignment of these myofibrils within each individual muscle fibre (McMahon, 1984; Lieber, 2002; Hall, 2011). The contractile unit in skeletal muscle tissue is the sarcomere. Thick filaments are primarily composed of the protein myosin, while thin filaments contain the protein actin.

Individual myofibrils within muscle fibres are surrounded by an intracellular membrane network known as the sarcoplasmic reticulum (SR). This structure plays a vital role in muscle contraction by regulating intracellular calcium (Ca^{2+}) levels. Ca^{2+} -dependent interaction of actin and myosin is the molecular basis resulting in muscle contraction and force generation (Plowman, 2017). Myosin plays a role in pulling thin filaments towards the centre of the sarcomere.

The central nervous system controls skeletal muscle contraction. The activity of alpha motor neurons which synapse on skeletal muscle fibres is regulated by motor centres in the brain. These motor centres are responsible for controlling motor neuron activity in the ventral horns of the spinal cord (Gransee *et al.*, 2012). For skeletal muscle contraction to occur, motor neurons must fire an action potential to cause the alpha motor neuron release of acetylcholine. A conformational change in the dihydropyridine receptors (DHPRs) induces SR Ca^{2+} channel (ryanodine receptor) opening, which results in increased myoplasmic Ca^{2+} concentrations. This increase promotes muscle contraction through the exposure of myosin binding sites on thin

filaments. When myoplasmic Ca^{2+} is sequestered by Ca^{2+} ATPase in the SR, relaxation occurs. Excitation–contraction coupling (ECC) describes the rapid communication between electrical events occurring in the plasma membrane of skeletal muscle fibres and Ca^{2+} release from the SR. The prolonged elevation of intracellular Ca^{2+} results in sustained muscle contraction.

1.1.1 Muscle Fibre Types

Skeletal muscle fibre types can be classified based on their individual speed of contraction, myosin ATPase activity and enzymatic activity along the various glycolytic and oxidative pathways. The two basic skeletal muscle fibre types are fast twitch (type IIA & type IIB) and slow twitch fibers (type I). Myosin isoform expression dictates the speed of contraction as this influences ATPase activity. These fibres also differ in motor unit size, fibre diameter, metabolic activity, recruitment pattern and sensitivity to tetany (increased muscle tension due to repeated stimulation). Slow-twitch muscle fibres are typically recruited first, before fast-twitch muscle fibres, due to the greater excitability of the neurons which innervate them. Slow-twitch fibres also have a high oxidative capacity which supports sustained contractile activity. On the other hand, fast-twitch fibres typically have a high glycolytic capacity and a low oxidative capacity. For short periods of activity where high levels of force are required, the fast twitch fibres are better suited. Mitochondrial expression is believed to play a role in influencing enzymatic activity. Following denervation, skeletal muscle fibres typically atrophy. Muscle fibres rely on motor nerve activity for the maintenance of muscle fibre size. Skeletal muscle exhibits plasticity and regular growth of skeletal muscle occurs through the addition of more myofibrils and sarcomeres.

1.1.2 Respiratory Muscle

Each respiratory muscle serves to aid the primary function of the lungs, gas exchange. The lungs supply oxygen to the vasculature, and in exchange they remove carbon dioxide. Pump muscles are involved in ventilation (movement of air into the lungs), while airway muscles control both upper and lower airway calibre. Airway muscles comprise of skeletal (upper) and smooth (bronchi and trachea) muscles. Respiratory muscles can exhibit plasticity in order to functionally adapt to physiological stimuli

(Koeppen & Stanton, 2010; Gransee *et al.*, 2012). Both the anatomy and composition of the upper airway muscles play important roles in performing tasks such as breathing, swallowing and speech (van Lunteren *et al.*, 1987). Upwards of 20 different skeletal muscles have roles in both the control and maintenance of airway calibre (Boyd *et al.*, 2004).

1.1.3 Diaphragm

The diaphragm is the primary pump muscle involved in ventilation, critical in maintaining respiratory homeostasis. The thoracic diaphragm is a sheet of skeletal muscle which extends across the bottom of the thoracic cavity. This C-shaped structure of muscle and fibrous tissue divides the chest cavity from the abdominal cavity. Innervation of the diaphragm muscle is supplied by the phrenic nerve, which is formed from the cervical nerves C3, C4 and C5. Diaphragm muscle spindles provide sensory input to the central nervous system and in turn can modulate motor output to the diaphragm along the phrenic nerve (Nair 2017). While the central portion of the diaphragm sends sensory afferents via the phrenic nerve, the peripheral portions of the diaphragm send sensory afferents via the intercostal (T5–T11) and subcostal nerves (T12). This muscle has a mixed fibre type composition (55% slow, 24% fast glycolytic and 21% fast oxidative fibers) allowing it to be resistant to fatigue (Polla *et al.*, 2004). With the largest proportion of muscle fibres being slow, the diaphragm can remain one of the more active muscles in the body. Large diaphragmatic and external intercostal muscle contractions work in tandem to increase the size of the thoracic cavity and reduce intra-thoracic pressure, facilitating lung inflation.

1.1.4 Intercostal Muscles

Accessory muscles of breathing, such as the intercostal muscles have an important role in facilitating ventilation in health and disease especially during increased ventilatory demand. The intercostal muscle group encompasses a variety of muscles which are located between the ribs. These muscles serve to form and move the chest wall. Through contractions, these muscles expand and narrow the size of the thoracic cavity in order to facilitate breathing. The structure of these muscles is composed of three principal layers (each with different functions): 1) innermost intercostal muscle; 2)

internal intercostal muscle; 3) external intercostal muscle. External intercostal muscle facilitates quiet and forced inhalation. This layer of muscle is responsible for the elevation and bending of the ribs allowing them to open, thus expanding the dimensions of the chest cavity. The fibres of external and internal muscles run in opposite directions and are innervated by the ventral rami of thoracic spinal nerves. Intercostal arteries provide the blood supply, and the intercostal veins provide drainage.

1.1.5 Genioglossus

The genioglossus (GG) muscle plays a crucial role in both the defence and maintenance of upper airway patency (Remmers *et al.*, 1978). The GG is one of the paired extrinsic muscles of the tongue which is fan-like in shape. The GG begins at the mental spine of the mandible and its insertions are the hyoid bone and the bottom of the tongue. The GG is innervated by the hypoglossal nerve. The GG receives its blood supply from the sublingual branch of the lingual artery, a branch of the external carotid artery. If sensory input and/or motor output become compromised, collapse of the airway can occur due to upper airway muscle hypotonia.

1.1.6 Sternohyoid

In addition to the GG, the sternohyoid (SH) muscles are essential pharyngeal muscles which are responsible for maintaining upper airway patency (Roberts *et al.*, 1984; Van de Graaff *et al.*, 1984; van Lunteren *et al.*, 1987). These paired muscles connect the sternum and the hyoid bone and are located anterior and parallel to the trachea. During inspiration, upper airway dilator muscles exhibit phasic activity (Sauerland & Harper, 1976; Sherrey *et al.*, 1986; Wiegand *et al.*, 1990), while during expiration, upper airway constrictor muscles exhibit phasic activity (Kuna & Vanoye, 1997). Innervation of the SH is provided by the anterior rami of the 1st to 3rd cervical spinal nerves (C1 - C3) via the ansa cervicalis of the cervical plexus. The negative pressure generated by the diaphragm muscle during inspiration is sensed by mechano-receptors located in the upper airway, leading to increased activation of pharyngeal dilator muscles and increased tone of the upper airway musculature (Mathew, 1984). This is an important reflex for maintaining upper airway patency and mediating airflow for

gas exchange in the lungs. Occlusions of the airway seem to occur when there is reduced activity of pharyngeal dilator muscles (Remmers *et al.*, 1978). The SH muscles move the hyoid bone anteriorly which stabilizes the upper airway to prevent collapse and maintain patency. Sternohyoid muscles are primarily composed of fast (type II B) muscle fibers sensitive to fatigue (Attal *et al.*, 2000b). There is an inverse relationship between fatigue resistance and force production in muscle fibres (Schiaffino & Reggiani, 2011). There is a balance between the opposing actions of the diaphragm and upper airway pharyngeal muscle activity which must be finely regulated in order to maintain upper airway patency (Remmers *et al.*, 1978; Attal *et al.*, 2000a; White, 2005). Thus, if either of the key respiratory muscles are compromised in any way, respiratory homeostasis will be challenged.

1.2 Motor Units

1.2.1 Henneman's Size Principle

Neuromuscular control of respiratory muscle is ultimately dependent on the physiological properties and function of respiratory muscle motor units. A motor unit is comprised of a single motor neuron together with the skeletal muscle fibres that it innervates. A collection of motor units is known as the motor 'pool'. Different members of this motor pool work in tandem with one another to allow motor control of skeletal muscle (Sherrington, 1935). The multiple skeletal muscle fibres within a single motor unit are homogeneous (same muscle fibre type). When a motor unit is active, each fibre within the unit contracts producing an output of force. The number of muscle fibres innervated by a motor neuron varies from muscle to muscle; larger muscles typically contain a greater abundance of muscle fibres. Thus, the larger the number of muscle fibres, the greater the level of force generation.

Motor units are typically categorised based on their mechanical and fatigability characteristics (Mantilla & Sieck, 2003). The four motor unit types are as follows: 1) Type S – slow twitch, fatigue resistant; 2) Type FR – fast twitch, fatigue resistant; 3) Type Flnt – fast twitch, fatigue intermediate; and 4) Type FF – fast twitch, fatigable. In a similar fashion, muscle fibre types are also classified into four types based on myosin heavy chain composition or histochemical properties: 1) Type I (Slow oxidative, MHC

slow); 2) Type IIa (Fast oxidative/glycolytic, MHC_{2A}); 3) type IIb (Fast glycolytic, MHC_{2B}); and 4) type IIx (MHC_{2X}) (Mantilla & Sieck, 2003).

1.2.1 Henneman's Size Principle

Pre-motor neurons located in the medulla provide rhythmic excitatory input to phrenic motor neurons in the cervical spinal cord. The central nervous system is responsible for the recruitment of motor neurons, typically recruiting smaller units first. This is captured in Henneman's size principle (Henneman *et al.*, 1965), whereby Henneman and colleagues inferred that motor units are recruited in order of size, from smallest to largest. The magnitude of the load on the muscle determines the type of muscle fibres required and thus the motor units which require activation. Typically, small loads would first require the recruitment of slow twitch, low-force, fatigue-resistant muscle fibres. If necessary, these would be followed by the recruitment of the fast twitch, high-force, less fatigue-resistant muscle fibres which would typically be components of larger motor neurons.

1.2.2 Rate Coding & Recruitment

In terms of controlling the force output of respiratory muscle, the respiratory network employs two key mechanisms, motor unit spatial and temporal recruitment. Spatial recruitment involves the recruitment and activation of more motor units in order to produce a greater output of force. On the other hand, temporal recruitment, otherwise known as 'rate coding', speaks to the change in the frequency of activation of motor units.

1.3 Control of Breathing

The primary function of the respiratory system is to keep the partial pressure of carbon dioxide (PaCO_2), oxygen (PaO_2) and pH constant to maintain blood-gas homeostasis. Thus, it is crucial that sensory, central and motor signaling are constantly active. The integrated respiratory control system is composed of the central pattern generator (medulla), and central (medulla oblongata) and peripheral (aortic arch & carotid sinus) chemoreceptors. Peripheral chemoreceptors (carotid body) send afferent signals to the medulla via the carotid sinus nerve and the reflex response is evoked based on the levels of blood PaO_2 , PaCO_2 and pH.

1.3.1 Neural Control of Breathing

Controlled ventilation involves a high level of timing and co-ordination. Motor neurons driving the pump muscles (facilitating inspiration and expiration) are located at various levels in the spinal cord. The diaphragm is innervated by the phrenic nerve (C3-C5), intercostal muscles by motor neurons in the thoracic spinal cord (T1-T12), and the abdominal muscles by motor neurons within the thoracic and lumbar regions of the spinal cord (T4-L3). Motor neurons which innervate the upper airway muscles are typically located in the brainstem or upper cervical spinal cord. The larynx is innervated by the recurrent laryngeal nerves, pharyngeal muscles by the glossopharyngeal nerves and the pharyngeal branch of the vagus. The hypoglossal (XII) nerve innervates the GG muscle, which controls upper airway patency and governs tongue protrusion during inspiration, while the tensor veli palatini muscle (soft palate) is innervated by the mandibular branch of the trigeminal nerve and serves to maintain nasopharyngeal isthmus patency during inspiration.

During inspiration, a dynamic reciprocal action exists between the glottis and respiratory pump muscles. The pump muscles (diaphragm and intercostal) contract and the glottis dilates (abduction). Upper airway pharyngeal muscles contract and dilate the pharynx, and the tongue is pulled forward facilitating airflow. Upper airway muscle movements precede diaphragm contraction (recurrent laryngeal and XII nerve activity precedes phrenic activity). Timing and control of these muscles can be modified by sensory feedback. Quiet expiration is a passive, but braked mechanism. This allows air to move out slowly, allowing a smoother transition between inspiration and expiration and mediating phonation. Diaphragm motor units can adapt to stimuli, by mediating an increase or decrease in motor unit activity. Remodelling of the neuromuscular system can lead to structural and physiological changes within the respiratory system. Motor neuron remodelling can occur also, such as dendritic branching or changes in somal surface area. Neuromuscular junction remodelling can occur, such as alterations at the pre- and post-synaptic membrane. In terms of myofibre remodelling, alterations in structural, mechanical and biochemical properties can occur. Adaptation or remodelling of the respiratory control system can be captured under the umbrella term of respiratory plasticity.

1.4 Respiratory Plasticity

Plasticity can be described as the ability of an organism to make significant changes to itself based on its environment or external stimuli. Building on this, respiratory plasticity can be defined as the persistent change in the respiratory neural control network based on a prior experience (Johnson & Mitchell, 2002; Mitchell & Johnson, 2003). These changes may involve functional and/or compositional adaptations. Recently, neuroplasticity has been considered as one of the building blocks of the respiratory control network (Feldman *et al.*, 2003; Mitchell & Johnson, 2003), especially when considering pathophysiological conditions. In recent years, the field has explored the potential of harnessing both spontaneous and induced respiratory plasticity for the treatment of clinical disorders in which ventilatory control is impaired (Gonzalez-Rothi *et al.*, 2015). The 'crossed phrenic phenomenon' demonstrates the phenomenon whereby the partial spontaneous functional recovery of phrenic motor output occurs post spinal hemi-section (Goshgarian, 2003). This has then been further examined after repeated cycles of chemostimulation through bouts of intermittent hypoxia (Vinit *et al.*, 2009; Dale-Nagle *et al.*, 2010; Lovett-Barr *et al.*, 2012).

Remarkably, spontaneous compensatory neuroplasticity is observed in animal models of clinical disorders such as motor neuron disease. In the rat model of amyotrophic lateral sclerosis (ALS), despite profound phrenic motor neuron death, a capacity to generate adequate tidal volume remains (Nichols *et al.*, 2013). Motor neurone disease is a neurodegenerative disorder which is characterised by progressive neuronal atrophy, muscle weakness and paralysis (Mayeux *et al.*, 2003). In terms of the respiratory system in ALS, motor neuron loss is a hallmark feature (Lyall *et al.*, 2001). It is not surprising that patients with ALS suffer from significant ventilatory impairment and obstructive sleep apnoea (Fallat *et al.*, 1979; Lyall *et al.*, 2001; Stewart *et al.*, 2001; Talakad N *et al.*, 2009). Of note, this respiratory insufficiency does not truly develop until the later stages of disease progression which begs a lot of questions. Currently, it is not understood whether this respiratory insufficiency occurs due to the late onset of motor neurone death or not. Animal models of ALS display convincing evidence that breathing functional capacity is preserved until well after respiratory motor neuron atrophy has developed (Nichols *et al.*, 2013). It has been seen at both human and

animal model level that despite significant neuropathology, and ultimately compromised phrenic motor output, breathing is still maintained. This considers the idea that intricate compensatory strategies must be at play in a do or die adaptation to preserve breathing capacity (Nichols *et al.*, 2013; Nichols *et al.*, 2015). The authors suggest that this strategy may have a four-pronged approach as follows: 1) enhanced central drive to functioning motor neurons; 2) active plasticity within said neurons; 3) enhanced plasticity at the level of the neuro-muscular junction (NMJ); and 4) alteration of demand from the diaphragm to less-used respiratory motor neuron pools.

1.4.1 Central Drive Plasticity

While inspiratory pattern formation and rhythm generation occurs at one location, in the ventrolateral medulla (Feldman *et al.*, 2013), the regulation of central respiratory drive to respiratory motor units may occur at many sites. Central respiratory drive may be manipulated by various afferent sensory inputs (Feldman *et al.*, 2013), such as carotid chemoreceptors (Kumar & Prabhakar, 2012), and pulmonary stretch receptors (Brouns *et al.*, 2012). Central respiratory drive may be increased or reduced from sensory feedback at the level of the spinal cord (Aminoff & Sears, 1971). Muscle spindles respond to changes in muscle velocity and length. By invoking the myotatic reflex respiratory muscle spindles can protect the body from overstretched induced injury. These spindles stimulate reflexively a muscle contraction and maintain muscle tone in order to prevent fibre damage. Repeated stimulation of central or peripheral chemoreceptors can sometimes maintain an adequate level of breathing in disease states.

1.4.2 Phrenic Motor Neuron Plasticity

There are two forms of inducible spinal respiratory plasticity: 1) Phrenic motor facilitation and 2) phrenic long-term facilitation. These exhibit clear signs of augmented synaptic inputs to respiratory motor neurons (Dale-Nagle *et al.*, 2010). In animal models of spinal cord injury, following acute intermittent hypoxia, phrenic long-term facilitation has shown the potential to increase phrenic motor output, improving respiratory motor neuron function. Furthermore, in animal models of contusion injury, a greater capacity for compensatory respiratory plasticity has been observed (Golder

et al., 2011; Lane *et al.*, 2012). In these rodents, despite mid-cervical spinal injury with severe phrenic motor neuron impairment, breathing capacity resumes to normalised levels. This supports the idea of compensatory respiratory strategies outside the realms of brainstem control and/or motor neuron plasticity.

1.4.3 Neuromuscular Junction Plasticity

Respiratory plasticity may occur at various sites, including downstream of the respiratory motor neurons (Mantilla & Sieck, 2003). Hallmark features of neuromuscular and neurological disorders include NMJ deterioration and muscle fibre atrophy and necrosis. These pathologies may be as a result of, or worsened by, neuronal degeneration (Krakora *et al.*, 2012). It is possible that compensatory mechanisms may be at play to delay this NMJ deterioration for as long as possible. Decreased action potentials and denervation is seen in rodent models of cervical contusion injury. Yet, remarkably, just 14 days after injury, there are signs of partial re-innervation of diaphragm fibres (Nicaise *et al.*, 2012). Structure-activity dynamics also exist between diaphragm muscle fibres and NMJs. Further to this, the recruitment of phrenic motor units may vary amongst a variety of behaviours (Mantilla & Sieck, 2011). There is evidence to suggest that respiratory plasticity at the level of the NMJ may play a key role in preserving respiratory capacity. However, this may be limited to the type of fibres/NMJ injured.

1.4.4 Plasticity - Shifting the demands of respiratory motor neuron pools

The final form of plasticity involves shifting the demands to other respiratory motor neuron pools. This shift may include the rotation of the demand to lesser compromised motor neuron pools or muscle fibres. This may involve switching from primary pathways (diaphragm) to other accessory pathways. It is established that intercostal muscles can maintain quiet breathing without diaphragm support (Maskrey *et al.*, 1992). Building on this, enhanced intercostal electromyogram (EMG) activity has been demonstrated in animals with bilateral phrenectomy, showing a possible mechanism of compensatory plasticity (Rice *et al.*, 2011) during times of compromised diaphragmatic function. Additionally, intercostal motor plasticity is greater compared to phrenic motor plasticity in response to episodic hypoxia (Fregosi & Mitchell, 1994).

This opens the possibility for targeting and harnessing respiratory neuronal plasticity via accessory pathways in order to facilitate breathing in neuromuscular and neurological disease.

1.5 Dystrophin

The dystrophin gene is currently the largest described human gene with its full-length RNA expression found mainly in skeletal and cardiac muscle with small amounts also being found in the brain (Falzarano *et al.*, 2015). In total, the dystrophin gene spans greater than 2.5 million base pairs, making it close to 0.1% of the entire human genome (Muntoni *et al.*, 2003). The structural protein dystrophin serves to anchor the extracellular matrix to the actin cytoskeleton via a protein complex spanning the sarcolemma. Dystrophin protects the sarcolemma from damage during muscle contraction and stress via F-actin binding to β -dystroglycan, with this interaction it can act as both a bridging and an anchoring protein (Cirak *et al.*, 2011; Ogura *et al.*, 2014). Dystrophin is part of a larger complex of proteins, making up the dystrophin associated protein complex (DAPC). When dystrophin is not present, muscle contraction places mechanical stress on the plasma membrane, which causes damage to muscle fibers in the absence of dystrophin and eventual necrosis (Gumerson & Michele, 2011). Muscle fibre regeneration does occur initially through satellite cells, however, when this regenerative capacity is exhausted (Ogura *et al.*, 2014), fibrosis prevails and fatty tissue infiltrates which results in the loss of functional myofibres (Cros *et al.*, 1989; Cirak *et al.*, 2011).

1.5.1 Dystrophinopathies

Dystrophinopathies are a group of genetic conditions which can result in a spectrum of muscle weakness, varying from mild to severe. These disorders are inherited in an X-linked manner, meaning males are far more likely to experience symptoms in comparison to females. Duchenne muscular dystrophy (DMD) is characterised by profound skeletal muscle weakness and dilated cardiomyopathy. Becker muscular dystrophy (BMD) is another type of muscular dystrophy in which symptoms may present in a much milder form with a later onset compared to DMD. A longer life expectancy is typically seen in patients with BMD.

1.5.2 DMD

DMD is the most severe disorder of the muscular dystrophies (Emery, 1991) and has the highest incidence of the dystrophinopathies. It is one of the most common rare genetic diseases occurring in 1:3300 live male births (Scheuerbrandt *et al.*, 1986; Chung *et al.*, 2016). DMD is a fatal X-chromosome linked recessive disorder caused by the deletion or alteration of the dystrophin gene (Hoffman *et al.*, 1987). The dystrophin gene may be altered as follows: deletions (65%), duplications (6-8%), minor mutations (10%), and other re-arrangements. In patients with DMD, the dystrophin protein is not expressed. DMD is named after the term 'dystrophy', meaning degeneration from disease and from Guillaume Duchenne, a French neurologist (Parent, 2005). DMD is typically diagnosed at age four, when the initial symptoms begin to appear (Pane *et al.*, 2013). Despite extensive research into DMD, there is no effective treatment to date. Patients are commonly wheelchair-bound by age 12 (Wagner & Berry, 2008) and have a significantly reduced life expectancy (Yiu & Kornberg, 2008).

1.5.3 Pathophysiology of DMD

A key characteristic of DMD is the continuous degeneration and subsequent weakening of skeletal muscles, leading to physical disability (Yiu & Kornberg, 2008). In the human condition, weight bearing muscles are affected initially, with weakness developing in the proximal lower and then upper limbs, followed by weakness of distal lower and then upper limbs (Barohn *et al.*, 1998). Patients with DMD are known to have elevated levels of creatine kinase within their serum. These elevated levels may signify impaired integrity of the muscle sarcolemma permitting the leakage of key enzymes out of the muscle cells (Ozawa *et al.*, 1999; Allen & Whitehead, 2011).

In patients with DMD, the diaphragm muscle is weakened due to accumulation of adipose and connective tissue (De Bruin *et al.*, 1997). Force production is decreased (Beck *et al.*, 2006), and patients hypoventilate (Smith *et al.*, 1989b). Due to reductions in skeletal and cardiac muscle function, respiratory and heart failure are the most common causes of premature death in DMD (Wu *et al.*, 2014). Hypoventilation (Smith *et al.*, 1989b) and obstructive events (apnoea) often appear in patients during sleep

(Hill *et al.*, 1992; Barbé *et al.*, 1994). This can result in blood gas disturbances (Smith *et al.*, 1989a) and thus sleep can be a dangerous period for patients.

1.5.4 Sleep-disordered Breathing in DMD

Obstructive sleep apnoea (OSA) is the most common form of sleep disordered breathing (SDB). Characteristics of this syndrome include poor performance of the upper airway resulting in significantly reduced (hypopnoea) or the complete cessation (apnoea) of airflow (Eckert & Malhotra, 2008). DMD patients with upper airway muscle complications are extremely susceptible to OSA. Approximately 80% of DMD patients suffer from SDB and display signs of hypoventilation (Barbé *et al.*, 1994; Labanowski *et al.*, 1996).

Disruptions to airflow and breathing can result in blood gas disturbances such as hypoxaemia (low O₂ in the blood) and hypercapnia (high CO₂ in the blood) (Krieger *et al.*, 1989). Collapse of the airway is due to a sleep-related reduction in upper airway muscle activity linked with consequent failure of the pharyngeal dilator muscles. These dilator muscles oppose the collapsing pressure that is generated by the diaphragm and accessory muscles during inspiration (Bradford *et al.*, 2005). Central and peripheral chemoreceptors (carotid bodies) recognise blood-gas disturbance and patients are forced to arouse from sleep to reinstate the obstructed airway. This leads to repetitive hypoxia/ reoxygenation cycles and disrupted sleep. This may occur several times per hour during sleep. A tight relationship exists between sleep-related disturbances and patients with muscular disorders. It is often the case that patients suffering from sleep-related disturbances will die at night (Barbé *et al.*, 1994). Barbé *et al.*, (1994) reported that sleep-related disturbances occur frequently in DMD patients. They suggest that sleep-related disturbances should be considered by physicians if diurnal arterial hypoxemia is present in older DMD patients.

The key comorbidities associated with DMD, namely, hypertension, diabetes, oxidative stress, and cardiovascular disease among others are also associated with OSA. Patients with OSA often complain of being overtired due to their fragmented sleep patterns. A variety of treatment options exist in relation to OSA such as weight loss, positive airway

pressure, oral appliances and surgery. Continuous positive airway pressure (CPAP) is widely considered to be the gold standard treatment for OSA. CPAP delivers a fixed constant pressure on inspiration and expiration and this increase prevents airway collapse during inspiration.

1.6 Models of Duchene Muscular Dystrophy

A variety of dystrophic animal models exist across a broad spectrum from rodent to canine models such as the dystrophic golden retriever (Ambrósio *et al.*, 2009), the dystrophic worm and the dystrophic zebrafish (Grounds *et al.*, 2008).

1.6.1 Dystrophin Deficient *mdx* Mouse

The *mdx* mouse is the most widely studied animal model of DMD (Falzarano *et al.*, 2015). The C57BL/10ScSn-Dmd*mdx*/J colony arose due to a spontaneous mutation in the premature stop codon which terminated exon 23 of the dystrophin gene (Arechavala-Gomez *et al.*, 2010). Similar to the human condition, in *mdx* mice the dystrophin protein is not expressed (Bulfield *et al.*, 1984). For the past three decades, the *mdx* mouse has been used extensively to test potential therapeutic strategies and to investigate the pathophysiology associated with muscular dystrophy. Disease progression in the diaphragm of the *mdx* mouse is relatable to the human condition with extensive fibrosis (Stedman *et al.*, 1991; Gosselin & Williams, 2006) continuing until death (Huang *et al.*, 2009). *Mdx* skeletal muscle shows repetitive cycles of degeneration and regeneration of muscle fibres, similar to the human condition. This repair initiates at 2 weeks, peaking at 12 months and continuing indefinitely. Chronic inflammation is evident by the infiltration of inflammatory cells in both DMD patients and *mdx* mouse peripheral skeletal muscles (Grounds *et al.*, 2008). However, the extent of fibrosis and subsequent loss of function in limb muscles is less severe in *mdx* mice (Dangain & Vrbova, 1984). The reduction in the loss of functional muscle in *mdx* mice could be due to the presence and upregulation of utrophin (Falzarano *et al.*, 2014). In *mdx* mice, normal calcium homeostasis is altered, resulting in increased cytotoxic levels of Ca^{2+} in muscle cells (Fong *et al.*, 1990; Turner *et al.*, 1993). Repeated cycles of muscle degeneration and regeneration eventually lead to the exhaustion of satellite cells.

A study showed that at 8 weeks of age, there is a significant respiratory phenotype evident in the *mdx* mouse (Burns *et al.*, 2015). Behaving *mdx* mice hypoventilate compared to control mice (Burns *et al.*, 2015, 2017). At this young age, diaphragm (Burns *et al.*, 2017b; Burns *et al.*, 2019c) and upper airway muscle (sternohyoid) weakness is present in *mdx* mice (Burns & O'Halloran, 2016; Burns *et al.*, 2017a). Studies conducted by (Mosqueira *et al.*, 2013), examined the integrity of respiratory control mechanisms of *mdx* mice. Studies using whole-body plethysmography and phrenic nerve recordings showed that ventilatory chemosensory drive is blunted in *mdx* mice. Additionally, through molecular analysis of the carotid body, they showed that mRNA and protein expression of dystrophin is absent in carotid bodies from *mdx* mice (Mosqueira *et al.*, 2013). Interestingly, Burns *et al.* (2017) describe hypoactivity in *mdx* carotid body, a sensory deficit that may explain the persistent hypoventilation at rest.

In addition to the C57BL/10ScSn-Dmd*mdx*/J, the DBA/2 *mdx* mouse is a relatively new murine model of DMD. This variation of *mdx* mice displays a more severe dystrophic phenotype making it more akin to the human condition in terms of histopathology (Rodrigues *et al.*, 2016). These DBA mice are shown to have a shorter life span when compared to other *mdx* models and have a more severe muscle phenotype. DBA/2 mice also show signs of a reduction in muscle mass, increased fatty tissue accumulation and fibrosis (Fukada *et al.*, 2010). Studies have investigated the effects of experimental sleep apnoea on cardiac and respiratory function. Upon exposure to episodic hypoxia (EH) (as would happen during sleep), they noticed an increase in fibrosis of both the diaphragm and cardiac muscle in 18-month old mice (Chaudhari *et al.*, 2016). Their comprehensive study suggests that sleep apnoea and EH greatly impacts both on respiratory and cardiac function in muscular dystrophy.

1.7 Management of DMD

Unfortunately, there are not many therapeutic options or treatments available for this fatal disease. According to Yiu and Kornberg (2008) the only pharmacological intervention demonstrating efficacy to date are corticosteroids.

1.7.1 Corticosteroids

Prednisolone was shown to have anti-inflammatory effects in reducing macrophage, lymphocyte (Wehling-Henricks *et al.*, 2004), and eosinophil expression in skeletal muscle (Marques *et al.*, 2009). *Mdx* mice have given great insight into the positive effects and mechanisms of steroidal action in DMD, however, long term studies (>100 days) have shown considerable drawbacks to long term treatment with corticosteroids. Steroids have been the gold standard therapy in DMD since 1974 (Drachman *et al.*, 1974). Although steroids may show signs of slowing the progression of the disease, certain side effects are also associated with administration. Side effects of steroidal agents include metabolic and nutritional disorders, and gastrointestinal symptoms. Steroidal agents have also been shown to induce fibrosis of both skeletal and cardiac tissue (Sali *et al.*, 2012). Other side effects of steroidal treatment include short stature, obesity and cataracts (Schara *et al.*, 2001).

1.7.2 Utrophin

An alternative therapy is the up-regulation of the utrophin protein to replace dystrophin. Both utrophin and dystrophin share similarities in structural organization and protein binding properties. Both in DMD patients and *mdx* mice, the expression of utrophin is seen to be increased naturally in order to replace the absent dystrophin. Utrophin expression naturally increases with age in DMD making for an adequate substitute for dystrophin (Guiraud *et al.*, 2015) while also allowing for muscle repair through the continuity of the myotubes in *mdx* mice (Nakamura, 2015; Tinsley *et al.*, 2015). SMT C1100 is an orally administered drug developed by Tinsley, Robinson and Davies, (2015). This utrophin modulator has been through various successful clinical trials with positive and safe results.

1.7.3 Exon Skipping

Exon skipping is a promising genetic therapy which can restore functional dystrophin by coding the protein after the nonsense mutation. The use of antisense oligonucleotides to induce skipping of the selected exons resulted in functional dystrophin in *mdx* mice (Goyenvallé *et al.*, 2004). However, the practical application of this technique has initially been problematic and use of *mdx* tissue has proved very beneficial in monitoring the therapeutic and adverse effects of genetic therapies prior to clinical trials (Hoen *et al.*, 2006). Although exon skipping rescued dystrophin expression in *mdx* mice in both tibialis and extensor digitorum longus muscles, the effect was localised and temporary (Goyenvallé *et al.*, 2004). Moreover, restoration of dystrophin expression in *mdx* mice resulted in an immune response to the new protein and low expression levels necessitated weekly intravenous administration of 20-O-methyl phosphorothioates (Lu *et al.*, 2005). Nonetheless, use of the *mdx* mouse to optimise delivery techniques has been more promising, using 20-O-methylmodified bases (AOs), which are widely used to alter premRNA processing although the duration of dystrophin expression was limited and expression was low (McClore *et al.*, 2006).

1.8 Aims and Hypothesis

Duchenne muscular dystrophy is a severe progressive muscular disorder which often culminates in respiratory failure and premature death. To date, there is no cure for this disease. At just 8 weeks of age there is evidence of a respiratory phenotype in the *mdx* model. *Mdx* mice display signs of muscle fibre loss and NMJ remodelling. However, despite severe diaphragm muscle weakness, *mdx* mice display signs of preserved breathing capacity with the ability to enhance ventilation in response to chemostimulation (Burns *et al.*, 2017). Moreover, peak inspiratory pressure-generating capacity is preserved in 2-month old *mdx* mice despite profound diaphragm weakness (Burns *et al.*, 2019c). It has been suggested that neural compensatory mechanisms are at play in *mdx* mice in support of breathing capacity at least early in dystrophic disease (O'Halloran & Burns, 2018; Burns *et al.*, 2019c). Moreover, the loss of compensatory plasticity with advancing disease may explain the development of respiratory insufficiency in DMD (Burns *et al.*, 2019). The aim of this thesis was to examine respiratory muscle motor unit behaviour in diaphragm, intercostal and upper airway

muscle in the *mdx* mouse model of DMD. We sought to determine if there was evidence of adaptation in respiratory motor pathways in young *mdx* mice that compensates for established respiratory muscle weakness.

Chapter 2: Methods

2. Methods

2.1 Ethical Approval

Procedures on live animals were performed under licence in accordance with Irish and European directive 2010/63/EU following ethical approval by University College Cork (AEEC no. 2013/035). Experiments were carried out in accordance with guidelines laid down by University College Cork's Animal Welfare Body, and conform to the principles and regulations described by Grundy (Grundy, 2015).

2.2 Experimental Animals

Male wild-type (WT; C57BL/10ScSnJ; n=23) and *mdx* (C57BL/10ScSn-Dmd^{mdx}/J; n=23) mice were purchased from the Jackson Laboratory (Bar Harbor, ME, USA) and were housed at University College Cork's animal facility. Animals were housed conventionally in temperature- and humidity-controlled rooms, operating on a 12 h light:12 h dark cycle with food and water available *ad libitum*. Mice were studied at eight weeks of age. A thorough assessment of respiratory performance was performed, including measurements of breathing and ventilatory capacity in response to chemoactivation, recordings of thoracic inspiratory pressure and respiratory muscle EMG *in vivo* and respiratory muscle functional tests *ex vivo*.

2.3 Respiratory Flow Recordings in Conscious wild-type and mdx mice

2.3.1 Whole-body plethysmography

Whole-body plethysmography was used to assess respiratory flow in unrestrained, unanaesthetised mice. WT (n=10) and *mdx* (n=8) mice were introduced into plethysmograph chambers (Model PLY4211; volume 600ml, Buxco Research Systems, Wilmington, NC, USA) and were allowed an acclimation period typically lasting 40-60 minutes, with room air passing through each chamber (1L.min⁻¹).

2.3.2 Experimental Protocol

Following acclimation, during confirmed periods of quiet rest, a 20-minute baseline recording was performed in normoxia (FiO₂ = 0.21; balance N₂). This was followed by maximal chemoreceptor stimulation with hypercapnic-hypoxia (FiO₂ = 0.10 & 6 FiCO₂=

0.06) for 5 minutes, to examine peak ventilatory capacity. Respiratory parameters including respiratory frequency (f_R), tidal volume (V_T) and minute ventilation (V_E) were recorded on a breath-by-breath basis for analysis offline.

2.3.3 Data Analysis

Baseline normoxic ventilation was determined as an average of the baseline period. For hypercapnic-hypoxia, ventilatory measurements were taken during the final (5th) minute of the challenge. V_T and V_E , were normalised for body mass (g).

2.4 Respiratory EMG and motor unit recordings in anaesthetised mice

2.4.1 Surgical Preparation

Animals were anaesthetised with 5% isoflurane in 60% O₂ (balance N₂). Male WT (n = 13) and *mdx* (n = 14) mice were immediately placed on a thermostatically-controlled heating blanket in the supine position and body temperature was maintained at 37°C as monitored via a rectal probe (Harvard Apparatus, Holliston, MA, USA). Animals were then weaned off isoflurane whilst urethane anesthesia was administered (1.7 g kg⁻¹ i.p.). Mice were maintained under urethane anesthesia for the remainder of the protocol. Assessment of an adequate depth of anesthesia was performed through the absence of the pedal withdrawal reflex in response to a noxious paw pinch. A pulse oximeter clip (MouseOx, Starr Life Sciences Corporation, Oakmount, PA, USA) was placed on the thigh of each mouse for the continuous measurement of peripheral O₂ saturation (S_PO₂). To avoid upper airway occlusion during surgery and throughout the protocol, a mid-cervical tracheotomy was performed. Using an electronic gas mixer (CWE Inc.), animals were maintained on supplemental O₂ (FiO₂ = 0.60; balance N₂) via a bias flow over the tracheal cannula opening.

2.4.2 Experimental Protocol

Following surgical preparation, animals were allowed to stabilize for ~10 minutes. Next, a steady-state baseline period was recorded for 10 minutes. Next, a hypercapnic-hypoxia (FiO₂ = 0.15; FiCO₂ 0.06; balance N₂) challenge was performed. Upon completion of the protocol, mice were euthanised via anaesthetic overdose.

2.4.3 Intramuscular EMG Recordings

Concentric needle electrodes (26G; Natus Manufacturing Ltd, Gort, Ireland) were inserted into the costal diaphragm, external intercostal (T3) and genioglossus muscles for the continuous measurement of EMG activity and motor unit potentials. Right-sided costal diaphragm recordings were made by blind insertion of the recording electrode under the lower ribcage guided by audio recording, which facilitated electrode placement into the muscle anchoring the beveled needle sufficiently to allow insertion of the recording electrode. Similarly, the intercostal electrode was placed using anatomical landmarks and inserted perpendicular to the ribs guided by audio recording. For the genioglossus, the needle electrode was inserted just lateral to the lingual frenulum via the floor of the mouth into the body of the muscle, once again guided by audio recordings. This standardized approach typically led to the identification of phasic motor activity upon first placement, and thereafter subtle movement of the electrode, guided by audio recordings, ensured close proximity of the electrode to active motor units. Each signal was amplified ($\times 5000$), filtered (500 Hz low cut-off to 5000 Hz high cut-off) and integrated (50 ms time constant; Neurolog system, Digitimer Ltd, Welwyn Garden City, UK). All signals were passed through an analog-to-digital converter (r8/30; ADInstruments) and motor unit potentials were acquired using Spike2 software (Cambridge Electronic Design Limited, UK). A critical parameter for the acquisition of action potential waveforms is a high sampling rate. For these motor unit recordings, a sampling rate of 12,500Hz was used. A reference electrode was placed in the gastrocnemius muscle of the right hind-limb.

2.4.4 Motor Unit Spike Sorting

The objective of motor unit sorting was to take a voltage trace consisting of action potentials from a multiplex of myocytes and characterize distinct, phasically-active and reproducible single motor unit potentials. In principle, the spikes fired by a single neuron tend to have a particular shape mainly determined by the orientation and distance relative to the site of recording, and the morphology of its dendritic tree. To sort motor units, we adapted the method of spike-sorting algorithms which have four main steps: i) filtering; ii) spike detection; (iii) feature extraction; and (iv) clustering.

2.4.4.1 Filtering

For the raw signal, spikes typically exist side-by-side with local field potentials (LFPs). The filtering step allowed us to separate both high and low frequency activity. To facilitate spike detection, a band-pass filter was used to set an amplitude threshold for incoming spikes. If values for the threshold were set too high, low amplitude spikes would be missed, and *vice versa* if the threshold was set too low, it would result in the excessive detection of false positive events e.g. background noise.

2.4.4.2 Detection

Spikes as well as background noise were visualised concurrently within the raw signal. To separate spikes from noise, strict detection functions were applied, and data windows were extracted to determine new and held units (see Table 2.1).

2.4.4.3 Feature Extraction

Principal component analysis (PCA) was used to extract features of the detected spikes. PCA uses orthogonal vectors to examine and display the directions of the largest instances of variability within the waveform. These variations are then represented as a linear combination of the principal components. This multifaceted and most commonly used approach examines features such as: (i) peak amplitude; (ii) trough amplitude; (iii) crest to crest trough amplitude; (iv) width; (v) rise slope; (vi) fall slope; (vii) energy/power/root mean squared (RMS). In principle, the greater the number of discriminative features examined, the better the ability to distinguish distinct spike shapes.

2.4.4.4 Clustering Analysis

The fourth and final step of our spike sorting algorithm was *K*-means clustering. *K*-means clustering aims to find similarities within the data set with the variable *K* given as the number of groups.

2.4.4.5 Data Analysis

For integrated diaphragm, intercostal and genioglossus EMG activity, amplitude was analysed and averaged during stable baseline periods, immediately prior to and during

chemostimulation with hypercapnic-hypoxia. Integrated EMG activity is expressed in arbitrary units (AU) and was compared between WT and *mdx* preparations. Modal instantaneous firing frequencies of the discriminated active single motor units were expressed in Hz and were compared between WT and *mdx* mice.

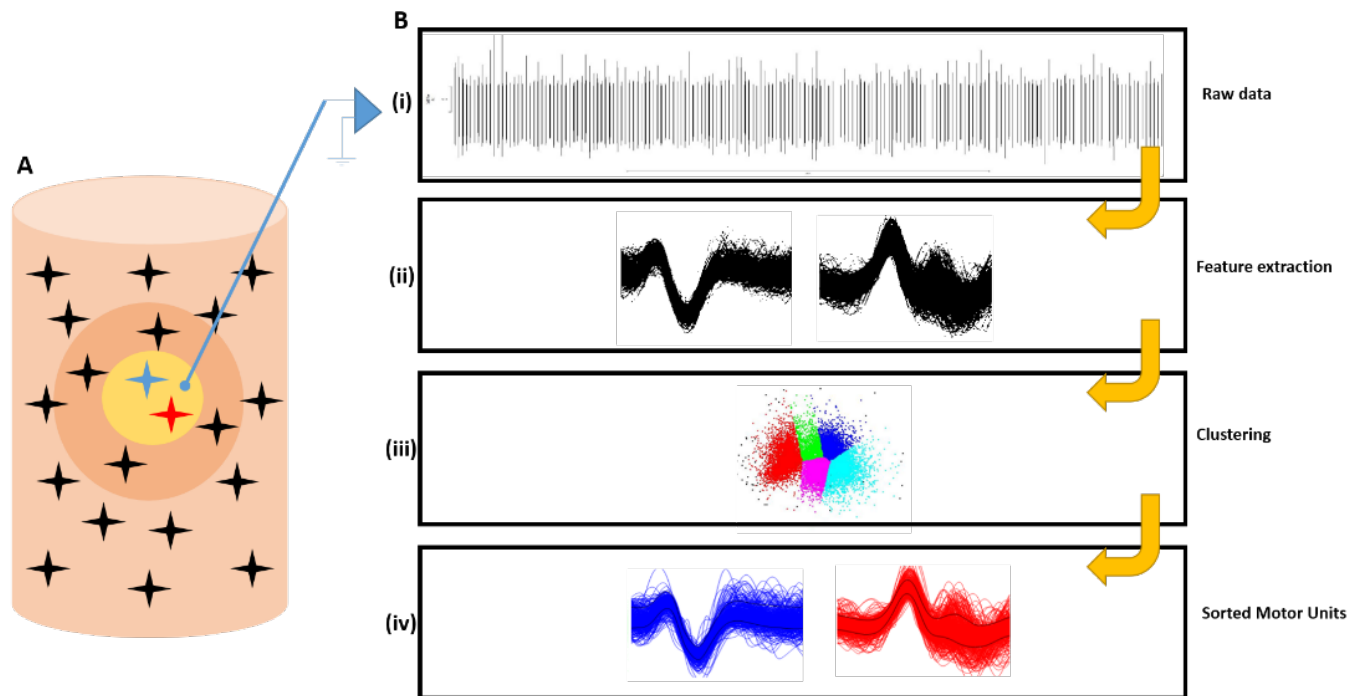


Figure 2.1. Intramuscular EMG recording and spike sorting process.

A) The electrical activity of myocytes recorded by concentric needle electrodes within the end effector muscle of interest. Blue and red motor units are within the range of detection and can be distinguished via offline spike sorting analysis. Black potentials are unsorted motor units which can be detected but are outside the spike sorting range.

(B) The four-step algorithm process used in spike sorting.

Section	Parameter	Definition	Set value
Forming a new template:			
	Number of similar spikes for a new template	Dictates how many spikes must match each other before a template is promoted from provisional status to one we can see and use for sorting	8
	Template width as a percentage of amplitude	Modifies the initial boundaries or limits of all templates.	32
	No template for shapes rare than 1 in N	If no spikes occur again within 1 in N count then the provisional template decays and may be deleted. This helps to avoid promoting spikes to 'real status' if they are very rare.	10
Matching a spike to a template:			
	Maximum percent amplitude changes for X	This helps if the spike class changes in amplitude and not shape.	0
	Minimum percentage of points in template	Specifies how many data points must lie within the boundaries of the template. If more than one template fits, then spikes are matched to the template with the smallest error between the mean template and the spike	
	Template modification mode	In this mode the first spike that forms the template has the most influence on the shape.	Add all
Waveform data section:		This is where we control how the raw waveform data is processed into spikes.	
	Waveform interpolation	Waveforms are shifted by fractions of a sampling interval to align them with templates using linear, parabolic or cubic spline interpolation.	Cubic spline
High-pass filter:		As a rule of thumb it should be set to approximately the width of the oscilloscope display. Too low a value will significantly change the spike shapes.	2.6ms
Remove DC offset before template matching:		This subtracts the mean level from each spike before matching. It is better to use the high-pass filter unless you have sudden DC shift in your baseline.	

Table 2.1. Detection functions, parameters, definition and set values considered for forming and holding motor unit templates.

2.5 *Ex vivo* Diaphragm Muscle Function

WT (n=10) and *mdx* (n=9) mice were anaesthetised with 5% isoflurane in $\text{FiO}_2 = 0.6$ (balance N_2) followed by gradual transfer to urethane anaesthesia (1.7g/kg i.p.). Following an *in vivo* assessment of respiratory performance, mice were euthanised by decapitation. The diaphragm muscle (rib and central tendon intact) was immediately excised and placed in a tissue bath at room temperature containing continuously gassed hyperoxic (95% O_2 / 5% CO_2) Krebs solution (in mM: NaCl, 120; KCl, 5; Ca^{2+} gluconate, 2.5; MgSO_4 , 1.2; NaH_2PO_4 , 1.2; NaHCO_3 , 25; and glucose, 11.5) and *d*-tubocurarine (25 μM) prior to functional analysis. Diaphragm muscle preparations were suspended vertically between two platinum plate electrodes in a water-jacketed tissue bath at 35°C containing Krebs solution and were continuously gassed with hyperoxia (95% O_2 & 5% CO_2). The rib was attached to an immobile hook and the central tendon was attached to a dual-mode force transducer (Aurora Scientific Inc.; Aurora, ON, Canada) with non-elastic string. Muscle optimum length (L_0) was determined by adjusting the position of the force transducer, in turn adjusting the length of the muscle preparations, using a micro-positioner between intermittent twitch contractions (Burns & O'Halloran, 2016; Burns *et al.*, 2017a). L_0 was determined as the muscle length which revealed maximal isometric twitch force in response to a single isometric twitch stimulation (supramaximal stimulation, 1ms duration). Preparations remained at L_0 for the duration of the protocol.

2.5.1. Experimental Protocol

A single isometric twitch contraction was measured. Peak isometric twitch force (P_t), contraction time (CT) and half-relaxation time ($\frac{1}{2}$ RT) were determined. The force-frequency relationship was examined by stimulating the muscle sequentially at 10, 20, 40, 60, 80, 100, 120, 140 and 160 Hz (300ms train duration). Contractions were interspersed by a 1 min interval. Next, an isotonic contraction was elicited in preparations at 0% load to examine maximum unloaded muscle shortening and velocity of shortening (Burns & O'Halloran, 2016; Burns *et al.*, 2017a).

2.5.2 Data Analysis

Muscle force was normalised for muscle cross-sectional area (CSA) and expressed as specific force ($\text{N}\cdot\text{cm}^{-2}$). The CSA of each muscle bundle was determined by dividing muscle mass (weight in grams) by the product of muscle L_0 (cm) and muscle density (assumed to be $1.06 \text{ g}\cdot\text{cm}^{-3}$). CT and $\frac{1}{2}$ RT were measured as indices of isometric twitch kinetics. Total muscle shortening was determined as the maximum distance shortened during contraction. Total muscle shortening (S_{max}) was determined in absolute units (cm) and was normalised to L_0 and expressed in L_0^{-1} . Shortening velocity (V_{max}) was measured as the distance shortened during the initial 30 ms of shortening (Lewis *et al.*, 2015; Lewis *et al.*, 2016; Burns *et al.*, 2017a) and was determined in absolute units ($\text{cm}\cdot\text{s}^{-1}$) and was normalised to L_0 and expressed in $L_0\cdot\text{s}^{-1}$.

2.6 Statistical Analysis

Data were statistically analysed by Prism 6.0 (Graphpad Software, San Diego, CA, USA). $P < 0.05$ was considered to be statistically significant; this was determined a priori. For measures of ventilation (Table 3.1), data are shown as mean \pm SD and were statistically compared using unpaired Student's *t* test with Welch's correction as appropriate, or Mann-Whitney test. For measures of EMG and motor unit properties (Figures 3.3, 3.4 and 3.5) data are presented as box and whisker plots (median, 25-75 percentile and scatter plot) and were statistically compared by unpaired Student's *t* tests or Mann-Whitney test. For measures of EMG (Figures 3.7, 3.8, 3.9) data are presented as box and whisker plots (median, 25-75 percentile and scatter plot) and were statistically compared by two-way ANOVA with Bonferroni post hoc test. For measures of *ex vivo* respiratory muscle contractile kinetics (Table 3.2) data are shown as mean \pm SD and were statistically compared using unpaired Student's *t* test with Welch's correction as appropriate, or Mann-Whitney test. For measures of *ex vivo* respiratory muscle contractile force (Figure 3.11), twitch and tetanic data were statistically compared using unpaired Student's *t* test with Welch's correction as appropriate, or Mann-Whitney test. Force-frequency data were statistically

compared using two-way ANOVA with Bonferroni post hoc test. * $P < 0.05$; ** $P < 0.01$;
*** $P < 0.001$; **** $P < 0.0001$.

Chapter 3: Results

3. Results

3.1 Baseline Ventilation and Ventilatory Responsiveness to Hypercapnic-Hypoxia in Conscious Mice

Figure 3.1 shows representative respiratory flow traces for wild-type (WT) and *mdx* mice during normoxia ($\text{FiO}_2 = 0.21$) and hypercapnic-hypoxia ($\text{FiO}_2 = 0.10$ & $\text{FiCO}_2 = 0.06$). Table 3.1 shows respiratory parameters including f_R , V_T and V_E during baseline ($\text{FiO}_2 = 0.21$) and hypercapnic-hypoxia. During baseline conditions, f_R was greater in *mdx* ($P = 0.0395$; unpaired Student's *t* test) compared with age-matched WT mice. Upon exposure to hypercapnic-hypoxia, V_T was lower in *mdx* ($P = 0.0343$) when compared with WT. Minute ventilation was equivalent for both groups during baseline conditions. There was a trend towards a reduction in minute ventilation for *mdx* mice ($P = 0.0711$) during hypercapnic-hypoxia compared to WT.

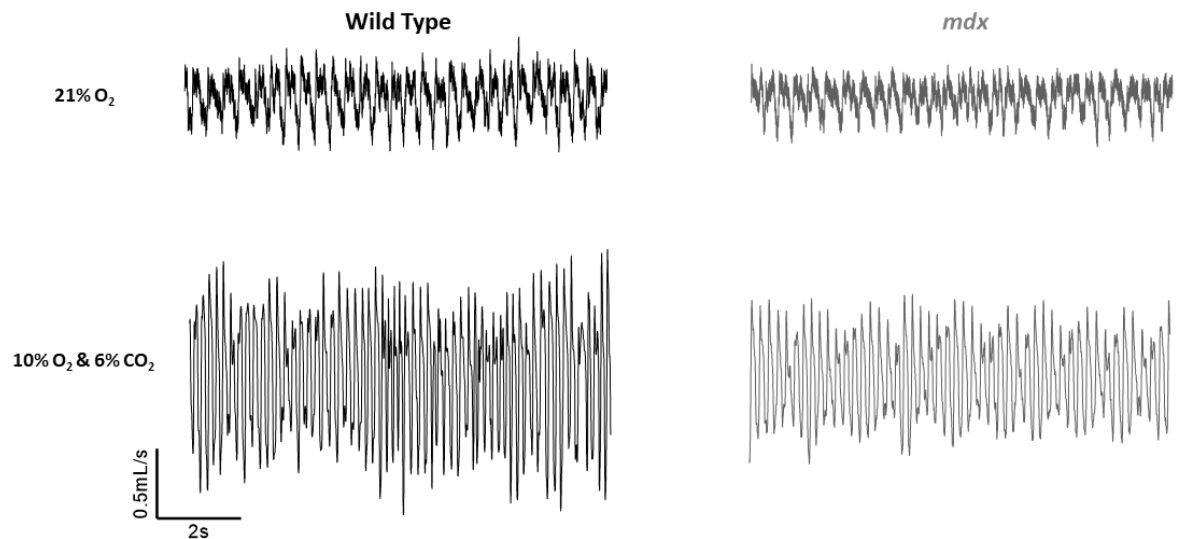


Figure 3.1. Respiratory flow traces.

Representative respiratory flow traces for WT (black) and *mdx* (grey) mice during normoxia ($\text{FiO}_2 = 0.21$) and hypercapnic-hypoxia ($\text{FiO}_2 = 0.10$ & $\text{FiCO}_2 = 0.06$). Inspiration downwards.

	WT	<i>mdx</i>	<i>P</i> value
	(n=10)	(n=8)	
Normoxia (21% O₂)			
<i>f_R</i> (brpm)	196 ± 15	211 ± 14	<i>P</i> = 0.0395
<i>V_T</i> (ml g ⁻¹ body mass)	0.007 ± 0.001	0.006 ± 0.001	<i>P</i> = 0.0959
<i>V_E</i> (ml g ⁻¹ min ⁻¹)	1.31 ± 0.15	1.28 ± 0.25	<i>P</i> = 0.6982
Hypercapnic-hypoxia (FiO₂ = 0.10 & FiCO₂ = 0.06)			
<i>f_R</i> (brpm)	366 ± 28	360 ± 61	<i>P</i> = 0.7726
<i>V_T</i> (ml g ⁻¹ body mass)	0.014 ± 0.002	0.011 ± 0.002	<i>P</i> = 0.0343
<i>V_E</i> (ml g ⁻¹ min ⁻¹)	5.01 ± 0.98	3.99 ± 1.24	<i>P</i> = 0.0711
Body mass (g)	24.8 ± 1.5	26.1 ± 0.8	<i>P</i> = 0.0382

Table 3.1. Breathing during normoxia and hypercapnic-hypoxia

Group data for breathing frequency (*f_R*), tidal volume (*V_T*) and minute ventilation (*V_E*) for WT (n=10) and *mdx* (n=8) mice during normoxia (FiO₂ = 0.6 ; balance N₂) and hypercapnic-hypoxia (FiO₂ = 0.1 and FiCO₂ = 0.06 ; balance N₂). Data are shown as mean ± SD and were statistically compared using unpaired Student's *t* test with Welch's correction as appropriate, or Mann-Whitney test.

3.2 Respiratory muscle motor unit properties

Figure 3.2 shows a representative trace of basal motor unit properties recorded from the GG muscle in an anaesthetised WT mouse using bipolar concentric needle electrodes.

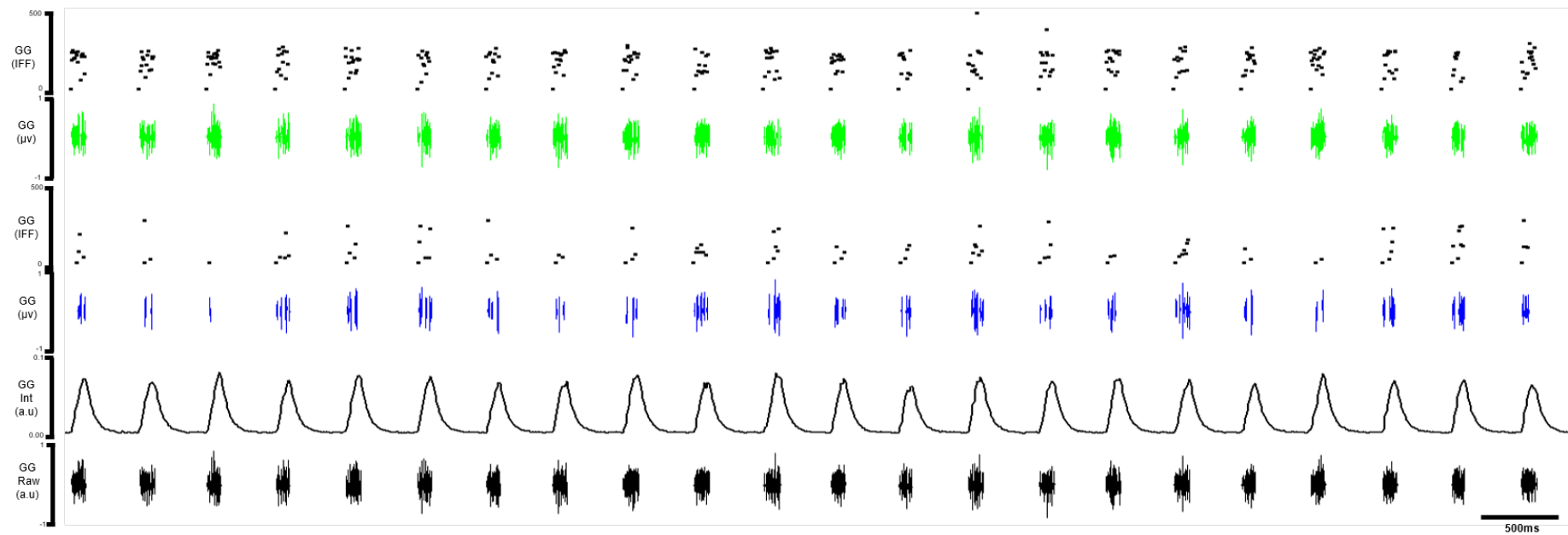


Figure 3.2. GG motor unit properties in an anaesthetised wild-type mouse.

Original traces of *in vivo* GG EMG and motor unit activities in anaesthetised WT mouse during baseline ($\text{FiO}_2 = 0.6$). The bottom black trace shows an original raw GG recording, with the integrated signal directly above. Both blue and green motor units were discriminated from the raw GG signal. Motor units are separated out showing their corresponding instantaneous firing frequencies.

3.2.1 Diaphragm

Diaphragm EMG activity during baseline was significantly lower in *mdx* (Fig. 3.3A; $P = 0.0031$; unpaired Student's *t* test) mice compared to WT. The number of diaphragm motor units active during baseline was significantly increased for *mdx* (Fig. 3.3.B; $P = 0.0075$; unpaired Student's *t* test) compared to WT. The instantaneous firing frequency (IFF) of diaphragm motor units was lower for *mdx* (Fig. 3.3C; $P = 0.064$; Mann-Whitney test) compared to WT.

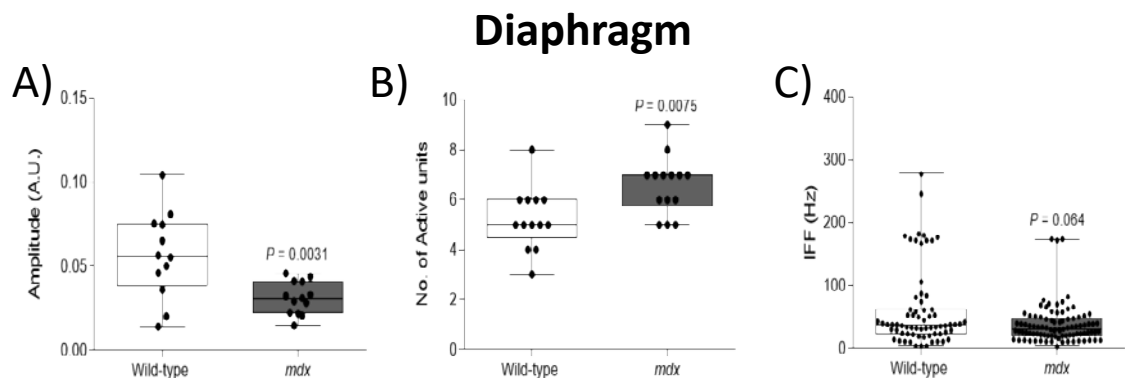


Figure 3.3. Diaphragm EMG and motor unit properties for anaesthetised mice during baseline conditions.

Group data for diaphragm EMG and motor unit properties for WT and *mdx* mice during baseline ($\text{FiO}_2 = 0.6$). A, B and C: Diaphragm EMG activity (A; amplitude), the number of active diaphragm motor units (B) and diaphragm instantaneous firing frequency (IFF) during baseline. Data are presented as box and whisker plots (median, 25-75 percentile and scatter plot) and were statistically compared by unpaired Student's *t* tests or Mann-Whitney test.

3.2.2 External Intercostal

External intercostal EMG activity during baseline was unchanged between WT and *mdx* mice (Fig. 3.4A; $P = 0.9235$; Mann-Whitney). The number of intercostal motor units active and the IFF of intercostal motor units were equivalent between WT and *mdx* mice (Fig. 3.4B & C; $P = 0.9323$ and $P = 0.7867$; unpaired Student's *t* test and Mann-Whitney; number of active units and IFF, respectively).

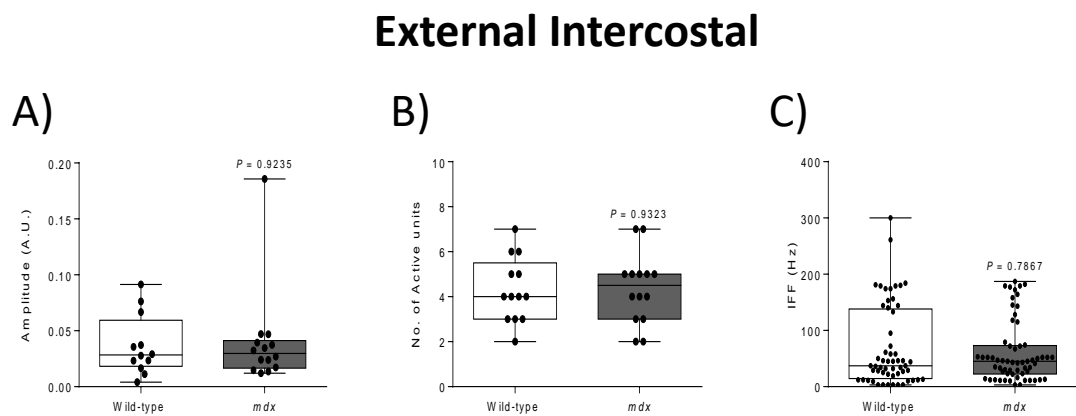


Figure 3.4. External intercostal EMG and motor unit properties for anaesthetised mice during baseline conditions.

Group data for external intercostal EMG and motor unit properties for WT and *mdx* mice during baseline ($\text{FiO}_2 = 0.6$). A, B and C: External intercostal EMG activity (A; amplitude), the number of active external intercostal motor units (B) and external intercostal instantaneous firing frequency (IFF) during baseline. Data are presented as box and whisker plots (median, 25-75 percentile and scatter plot) and were statistically compared by unpaired Student's *t* test or Mann-Whitney test.

3.2.3 Genioglossus

GG EMG activity during baseline was equivalent between WT and *mdx* mice (Fig. 3.5A; $P = 0.9173$; Mann-Whitney test). The number of GG motor units active during baseline was significantly increased for *mdx* (Fig. 3.5B; $P = 0.019$; Mann-Whitney test) compared to WT. Furthermore, no difference was observed for GG IFF between groups (Fig. 3.5C; $P = 0.7761$; Mann-Whitney).

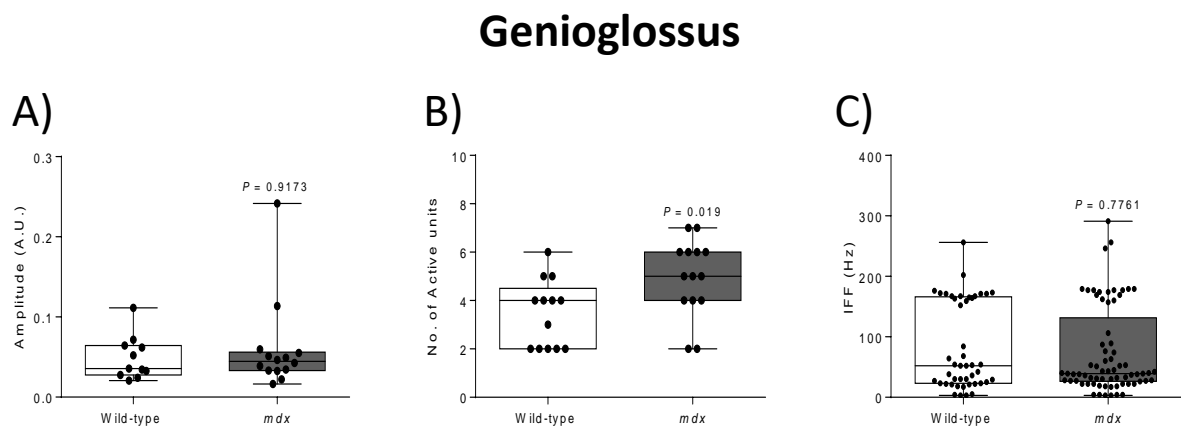


Figure 3.5. GG EMG and motor unit properties for anaesthetised mice during baseline conditions.

Group data for GG EMG and motor unit properties for WT and *mdx* mice during baseline ($\text{FiO}_2 = 0.6$) A, B and C: GG EMG activity Amplitude (A), the number of active GG motor units (B) and GG instantaneous firing frequency (IFF) (C) during baseline. Data are presented as box and whisker plots (median, 25-75 percentile and scatter plot) and were statistically compared by Mann-Whitney test.

3.3 Respiratory Muscle EMG Activity in Anaesthetised Mice During Baseline and Chemostimulation

Figure 3.6 shows representative original traces for diaphragm, intercostal and GG EMG activities during baseline ($\text{FiO}_2 = 0.6$) and chemostimulation with hypercapnic-hypoxia ($\text{FiO}_2 = 0.15$ & $\text{FiCO}_2 = 0.06$).

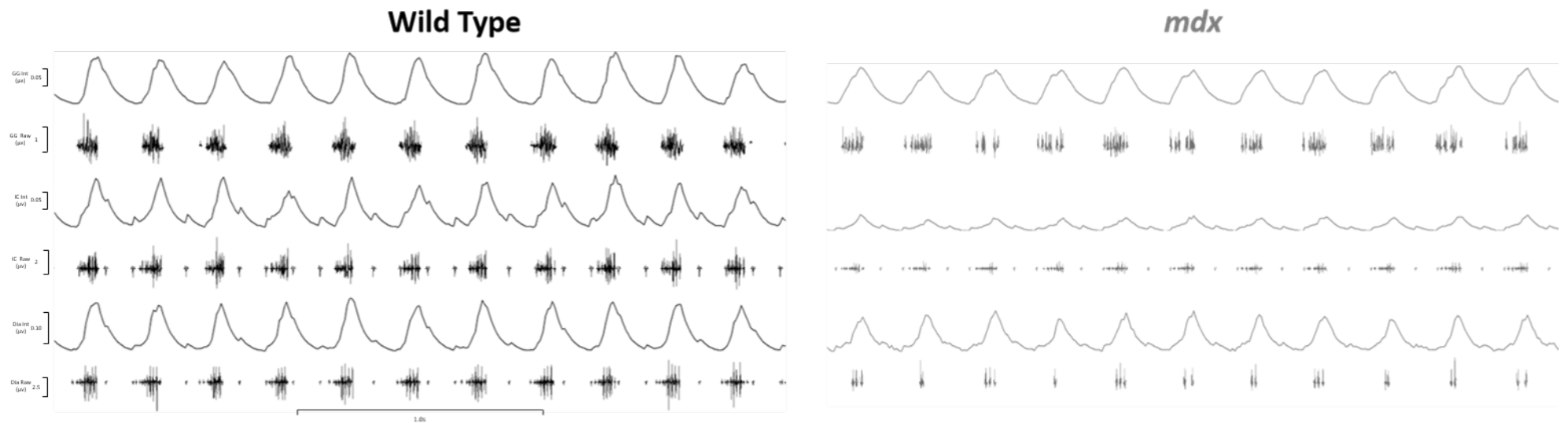


Figure 3.6. Diaphragm, intercostal and GG EMG activity in anaesthetised mice.

Original traces of diaphragm (Dia - bottom 2 traces), intercostal (IC - middle 2 traces) and GG (top 2 traces) EMG activities in anaesthetised WT (black) and *mdx* (grey) mice during baseline ($\text{FiO}_2 = 0.6$). For each muscle, the bottom trace shows an original raw recording, with the integrated signal directly above.

Chemostimulation with hypercapnic-hypoxia resulted in an increase in diaphragm (Fig. 3.7; $P < 0.0001$; repeated measures two-way ANOVA), intercostal (Fig. 3.8; $P < 0.0001$) and GG (Fig. 3.9; $P = 0.0573$) EMG activity. During hypercapnic-hypoxia, diaphragm EMG activity (amplitude) was significantly lower for *mdx* (Fig. 3.7; $P < 0.05$; repeated measures two-way ANOVA with Bonferroni *post hoc* test) compared to WT. During baseline and hypercapnic-hypoxia, external intercostal EMG activity was equivalent between WT and *mdx* mice (Fig. 3.8; $P = 0.4674$; two-way ANOVA (genotype)). Similarly, GG EMG activity was equivalent between WT and *mdx* mice (Fig. 3.9; $P = 0.5304$; two-way ANOVA (genotype)) during baseline and chemoactivation (hypercapnic-hypoxia).

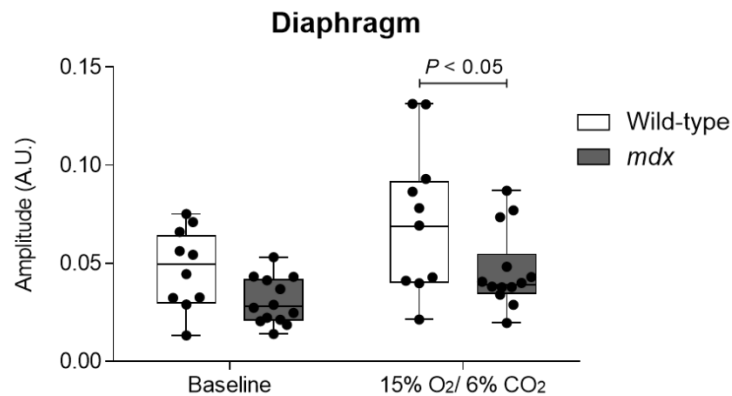


Figure 3.7. Diaphragm EMG activity in anaesthetised mice during baseline and hypercapnic-hypoxia.

Group data for diaphragm EMG activity during baseline ($\text{FiO}_2 = 0.6$) and chemostimulation with hypercapnic-hypoxia ($\text{FiO}_2 = 0.15$ / $\text{FiCO}_2 = 0.06$). Data are presented as box and whisker plots (median, 25-75 percentile and scatter plot) and were statistically compared by two-way ANOVA with Bonferroni *post hoc* test.

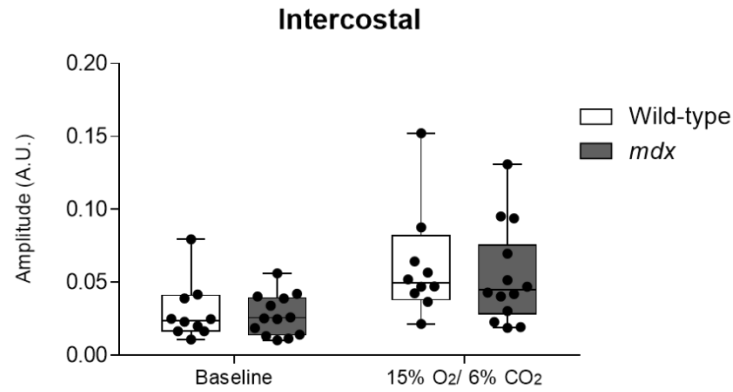


Figure 3.8. External intercostal EMG activity in anaesthetised mice during baseline and hypercapnic-hypoxia.

Group data for external intercostal EMG activity during baseline ($\text{FiO}_2 = 0.6$) and chemostimulation with hypercapnic-hypoxia ($\text{FiO}_2 = 0.15$ / $\text{FiCO}_2 = 0.06$). Data are presented as box and whisker plots (median, 25-75 percentile and scatter plot) and were statistically compared by two-way ANOVA with Bonferroni *post hoc* test.

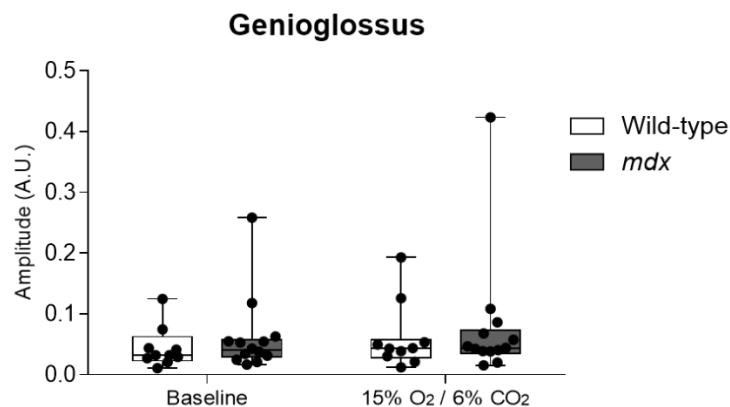


Figure 3.9 GG EMG activity in anaesthetised mice during baseline and hypercapnic-hypoxia.

Group data for GG EMG activity during baseline ($\text{FiO}_2 = 0.6$) and chemostimulation with hypercapnic-hypoxia ($\text{FiO}_2 = 0.15$ / $\text{FiCO}_2 = 0.06$). Data are presented as box and whisker plots (median, 25-75 percentile and scatter plot) and were statistically compared by two-way ANOVA with Bonferroni *post hoc* test.

3.4 Diaphragm Muscle Contractile Function *ex vivo*

Figure 3.10 shows representative original traces for diaphragm muscle twitch (A) and tetanic (B) contractions, force-frequency relationship (C) and maximum unloaded shortening (D). Table 3.2 shows data for twitch contractile kinetics (CT and $\frac{1}{2}$ RT) and isotonic contractile kinetics (S_{\max} and V_{\max}) of diaphragm muscle preparations from WT and *mdx* mice. Diaphragm CT and $\frac{1}{2}$ RT were equivalent in WT and *mdx* preparations. Absolute values for S_{\max} and V_{\max} were lower in *mdx* ($P = 0.0003$ and $P = 0.0117$ respectively; unpaired Student's *t* test and Mann-Whitney test) diaphragm preparations compared with WT. Normalised values for S_{\max} and V_{\max} were equivalent in both groups.

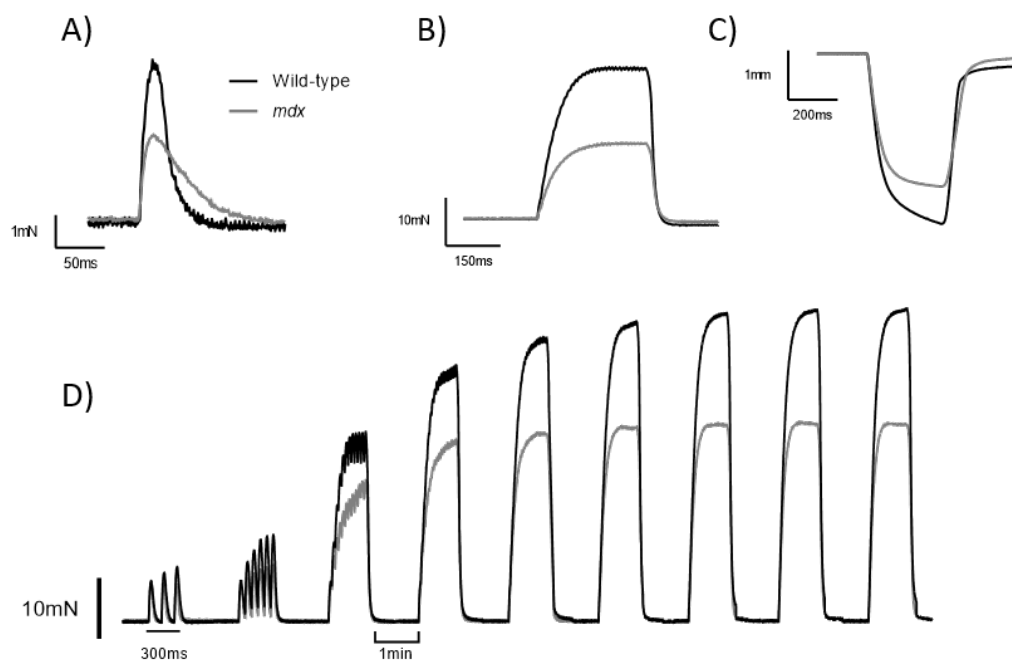


Figure 3.10. *Ex vivo* diaphragm muscle contractions.

A-D: original traces of *ex vivo* diaphragm muscle twitch contraction (A), tetanic contraction (B), maximum unloaded shortening (C) and force-frequency relationship (D) for WT (black) and *mdx* (grey) diaphragm preparations.

	WT (n = 10)	<i>mdx</i> (n = 8-9)	<i>P</i> value
CT (ms)	17.2 ± 2.6	18.1 ± 4.0	<i>P</i> = 0.5875
½ RT (ms)	19.9 ± 6.9	21.7 ± 9.0	<i>P</i> = 0.6357
Smax (cm)	0.39 ± 0.08	0.23 ± 0.06	<i>P</i> = 0.0003
Smax (L L _o ⁻¹)	0.37 ± 0.06	0.31 ± 0.08	<i>P</i> = 0.0772
Vmax (cm s ⁻¹)	4.1 ± 1.0	2.3 ± 1.2	<i>P</i> = 0.0117
Vmax (L _o s ⁻¹)	4.0 ± 1.0	3.2 ± 1.7	<i>P</i> = 0.237
L _o (cm)	1.1 ± 0.1	0.8 ± 0.1	<i>P</i> = 0.0003

Table 3.2. *Ex vivo* respiratory muscle contractile kinetics.

Definition of abbreviations: ½ RT, half-relaxation time; CT, contraction time; L_o, optimum length; Smax, maximum unloaded shortening; Vmax, maximum shortening velocity. Data are shown as mean ± SD and were statistically compared using unpaired Student's *t* test with Welch's correction as appropriate, or Mann-Whitney test.

Diaphragm twitch force was lower in *mdx* (Fig. 3.8A P_t ; $P = 0.013$; Mann-Whitney test) compared with WT. Diaphragm tetanic force at 100 Hz was lower in *mdx* (Fig. 3.8B, P_o ; $P < 0.0001$; Mann-Whitney test) compared with WT. For the force-frequency relationship, diaphragm specific force was reduced in *mdx* compared with WT preparations (Fig. 3.8B; $P < 0.0001$; repeated measures two-way ANOVA). *Post hoc* analysis revealed differences between WT and *mdx* diaphragm across a broad stimulus range (40-160 Hz).

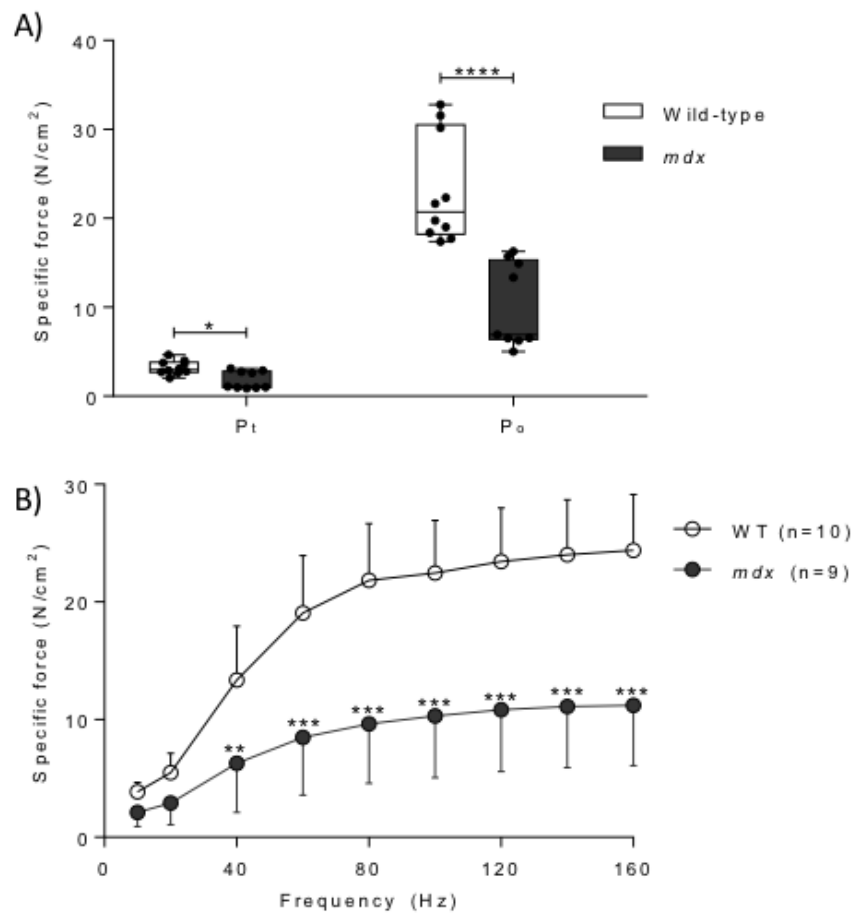


Figure 3.11. Ex vivo diaphragm muscle contractile force.

A & B, group data (mean \pm SD) for *ex vivo* diaphragm muscle twitch (A; P_t), tetanic (A; P_o) and force-frequency relationship (B) for wild-type (WT; black) and *mdx* (grey) muscle preparations. Twitch and tetanic data were statistically compared using unpaired Student's *t* test with Welch's correction as appropriate, or Mann-Whitney test. Force-frequency data were statistically compared using two-way ANOVA with Bonferroni *post hoc* test. * $P < 0.05$; ** $P < 0.01$; *** $P < 0.001$; **** $P < 0.0001$.

Chapter 4: Discussion

4. Discussion

The major findings of this thesis include: (1) diaphragm muscle function is severely impaired in young *mdx* mice; (2) despite substantial diaphragm muscle weakness, freely-behaving *mdx* mice can increase ventilation during chemostimulation with hypercapnic-hypoxia, indicating a significant ventilatory reserve; (3) motor unit recordings revealed altered motor unit properties for *mdx* mice as evidenced by an increase in the number of active units for diaphragm and genioglossus muscle (but not intercostal) and a reduction in the instantaneous firing frequency for diaphragm motor units compared to WT; and (4) diaphragm EMG activity was depressed in *mdx* mice during baseline and maximum chemostimulation, compared to WT.

Dystrophin is a cytoskeletal protein important for stabilizing the muscle sarcolemma. DMD is an X-linked recessive disorder which occurs due to mutation in the dystrophin gene. DMD initially manifests as muscle weakness due to a lack of expression of dystrophin protein (Yiu & Kornberg, 2008). In healthy muscle, dystrophin has a structural role in supporting muscle fibres during repeated cycles of muscle contraction, acting to limit the mechanical stress applied to muscle fibres (Ervasti & Campbell, 1991; Petrof *et al.*, 1993). In the absence of dystrophin, such as in DMD, skeletal muscle fibres have increased fragility resulting in fibre damage. Common pathological features of dystrophic muscle include myonecrosis, inflammation and oxidative stress (Deconinck & Dan, 2007; Petrillo *et al.*, 2017). Due to profound muscle weakness and damage, children with DMD have difficulty with ambulation in their early years, necessitating assistive devices.

In addition to dystrophin's role in muscle, dystrophin expression has been demonstrated in neuronal populations within regions such as the hippocampus (Lidov, 1996). Interestingly, the expression of dystrophin was reported in the carotid bodies of WT mice and absent within the carotid body of *mdx* mice (Mosqueira *et al.*, 2013). Despite dystrophin expression within the central nervous system, it is unclear if the neuromuscular control of dystrophic muscle is affected in individuals with DMD. Moreover, dystrophin has an important role in stabilizing the motor end plate (Pratt *et al.*, 2015).

A pathological feature of DMD includes respiratory muscle weakness, resulting in compromised respiratory function. Reductions in forced vital capacity (Mayer *et al.*, 2015; Meier *et al.*, 2017) and impaired inspiratory muscle strength are evident from a young age in DMD (De Bruin *et al.*, 1997; Khirani *et al.*, 2014). Respiratory system morbidity occurs in DMD due to weakness of the respiratory musculature (Khirani *et al.*, 2014; LoMauro *et al.*, 2017), the end effectors of breathing. Adequate respiratory muscle performance is essential for ventilation and mechanical manoeuvres including coughing and sneezing, and other protective mechanisms which safeguard against airway collapse. Inspiratory muscle strength declines with increasing age in DMD boys (Khirani *et al.*, 2014). Individuals with DMD are predisposed to an increased risk of respiratory disturbance during sleep, including hypoventilation (Smith *et al.*, 1989b; Kirk *et al.*, 2000) and central and or obstructive apnoeic events (Khan & Heckmatt, 1994; Suresh *et al.*, 2005; LoMauro *et al.*, 2017). Many DMD patients require ventilatory support during sleep to maintain blood gas homeostasis to prevent oxygen desaturation from occurring. Cough and airway clearance manoeuvres are compromised in DMD due to reduced respiratory muscle strength, such that patients are more susceptible to aspiration pneumonia (Toussaint *et al.*, 2016).

The *mdx* mouse is a dystrophin-deficient animal model of DMD. Skeletal muscle weakness occurs in *mdx* mice. Studies of the respiratory system in the *mdx* mouse have documented profound diaphragm muscle weakness and structural remodelling from a young age as a consequence of dystrophin deficiency (Stedman *et al.*, 1991; Coirault *et al.*, 1999; Coirault *et al.*, 2003; Burns *et al.*, 2017c; Burns *et al.*, 2019c). Structural changes include muscle fibres undergoing inflammatory cell infiltration, fibrosis and necrosis (Gayraud *et al.*, 2007; Ishizaki *et al.*, 2008; Huang *et al.*, 2011). Inflammatory markers such as cytokine concentrations are increased in *mdx* diaphragm, as well as the abundance of collagen deposits (Burns *et al.*, 2018; Burns *et al.*, 2019a). Moreover, indices of oxidative stress including lipid peroxidation and superoxide levels are elevated in *mdx* diaphragm compared with control muscle (Moraes *et al.*, 2015). Inflammation and high levels of reactive oxygen species (ROS) can culminate in skeletal muscle damage leading to poor physiological performance

(Reid, 2001). Impaired pharyngeal muscle function (sternohyoid) has been described in *mdx* mice (Attal *et al.*, 2000b; Burns & O'Halloran, 2016). Preserved diaphragm function and endurance is essential for performing ventilatory and non-ventilatory behaviors including coughing and sneezing (Sieck & Fournier, 1989). Moreover, adequate performance of the upper airway musculature is essential to maintain upper airway patency and to prevent collapse of the airway and disruption to airflow, that can lead to blood-gas disturbances.

Recent studies from our group have indicated altered sensory and motor control of dystrophic respiratory muscles in *mdx* mice (Burns *et al.*, 2017b; Burns *et al.*, 2019c). Our recent study reported lower diaphragm EMG activity in anaesthetised *mdx* mice during near maximal activation of the diaphragm (Burns *et al.*, 2019c). Moreover, we revealed a relative hypo-activity of the carotid body in *mdx* mice, which may influence eupnoeic breathing (Burns *et al.*, 2017b; Burns *et al.*, 2019b). Depressed diaphragm EMG activity during near-maximal activation in *mdx* mice is likely reflective of diaphragm neuromuscular junction impairment (Pratt *et al.*, 2015; van der Pijl *et al.*, 2016) and combined with intrinsic diaphragm muscle weakness reveals a major functional deficit in the diaphragm in muscular dystrophy.

In the current study, diaphragm muscle weakness in young *mdx* mice was evidenced by reduced twitch and tetanic force, consistent with previous reports in young and older *mdx* mice (Stedman *et al.*, 1991; Coirault *et al.*, 2003; Burns *et al.*, 2017b; Burns *et al.*, 2018; Burns *et al.*, 2019c). Specific force was reduced within the frequency range of 40-160 Hz for *mdx* diaphragm compared with WT. This frequency range corresponds to a broad range of ventilatory and non-ventilatory behaviours (Sieck *et al.*, 2013; Mantilla *et al.*, 2014; O'Halloran & Burns, 2018; Burns *et al.*, 2019c). S_{max} and V_{max} are lower in *mdx* and this is consistent with increased fibrosis within the diaphragm of *mdx* mice. Structural abnormalities occur in dystrophic muscle as a consequence of dystrophin deficiency and is further compounded by cycles of muscle fibre damage. Our previous study confirmed structural alterations in *mdx* diaphragm, including a substantial increase in the number of centralised myonuclei (measure of fibre regeneration following damage), increased expression of embryonic myosin

MyHC_{EMB} and increased collagen content (fibrosis) (Burns *et al.*, 2019a). These observations are consistent with and extend our previous findings (Burns *et al.*, 2017b; Burns *et al.*, 2018) and those of others (Barros Maranhão *et al.*, 2015; Gutpell *et al.*, 2015), revealing substantial diaphragm muscle pathology in young (8 week old) *mdx* mice.

Breathing was assessed using whole-body plethysmography in conscious mice during baseline ($F_{iO_2} = 0.21$) and chemoactivated breathing with hypercapnic-hypoxia ($F_{iO_2} = 0.10$ and $F_{iCO_2} = 0.06$). These assessments confirmed the capacity for *mdx* mice to enhance ventilation as previously described (Burns *et al.*, 2017c; Burns *et al.*, 2019c). Hypercapnic hypoxia is commonly used as a respiratory stimulant in studies utilizing pre-clinical models, including models of neuromuscular diseases such as DMD (Seven *et al.*, 2018; Burns *et al.*, 2019c). Hypoxia activates peripheral chemoreceptors (carotid bodies) and carbon dioxide activates both central and peripheral chemoreceptors, all of which leads to enhanced respiratory motor output (Kumar & Prabhakar, 2012). In response to hypercapnic-hypoxia, WT and *mdx* mice elevated ventilation by increasing respiratory frequency and tidal volume. Tidal volume generation during hypercapnic-hypoxia was lower in *mdx* compared with WT. Nevertheless, these experiments confirmed the capacity for *mdx* mice to boost ventilation in response to chemostimulation, consistent with our previous studies which examined the hypoxic and hypercapnic ventilatory response in young *mdx* mice (Burns *et al.*, 2017b; Burns *et al.*, 2019c). Interestingly, others have reported a loss of ventilatory responsiveness to hypercapnia with increasing age in *mdx* mice, suggesting a progressive decline in respiratory system function with disease progression (Gosselin *et al.*, 2003; Huang *et al.*, 2011; Mosqueira *et al.*, 2013).

Respiratory plasticity can be defined as the persistent change in the respiratory neural control network based on a prior experience (Mitchell & Johnson, 2003; Johnson & Mitchell, 2013). At both human and animal level, a respiratory breath is still achievable against all the odds despite significant neuropathology and compromised phrenic motor output. This suggests that compensatory strategies may be at play in order to preserve breathing capacity. Nichols and Mitchell suggest that

this may be a multi-faceted approach employed by the CNS: 1) Enhanced central drive to functioning motor neurons 2); active plasticity within said neurons; 3) enhanced plasticity at the level of the NMJ; and 4) alteration of demand from diaphragm to less-used respiratory motor pools (Nichols *et al.*, 2013).

Neuromuscular control of respiratory muscle contraction is ultimately dependent on respiratory muscle motor units. Our study is the first to assess the activity of respiratory muscle motor units in *mdx* mice. We recorded motor unit activity of the diaphragm, external intercostal and genioglossus muscles. We observed altered motor unit properties of the diaphragm compared to WT. This was evidenced by an increase in the number of active units, coupled with a lower instantaneous firing frequency. This is consistent with assessments of the myosin heavy chain (MyHC) isoform composition of diaphragm muscle samples from *mdx* mice (Burns *et al.*, 2018). These studies demonstrate a reduction in the number of diaphragm fibres expressing MyHC IIx and IIb. This reduction is coupled with an increase in the number of diaphragm fibres expressing MyHC I and IIa, indicating a higher number of oxidative fibres. For healthy neuromuscular systems, an increase in the number of active diaphragm motor units typically occurs during ventilatory challenge such as chemoactivated breathing i.e. motor unit recruitment. In disease states such as DMD, an increase in the number of active motor units during baseline conditions may indicate compensation within the respiratory neuromuscular system acting to facilitate adequate ventilation. An increase in the number of active diaphragm motor units would lead to relatively greater activation of *mdx* diaphragm muscle and may be reflective of sprouting and re-innervation of remodelled dystrophic muscle.

We anticipated that respiratory compensation in dystrophic disease would be characterised by an increase in the instantaneous firing frequency of *mdx* diaphragm during baseline. Such plasticity is observed to maintain respiratory performance in spinal cord injury (Nguyen *et al.* 2020). Unexpectedly, we observed a slight reduction in the instantaneous firing frequency of diaphragm motor units, which could occur for a number of different reasons: (1) a reduction in neural drive; (2) impaired transmission across the neuromuscular junction; and (3) a change in motor neuron

morphometry. Whatever the mechanism, this alteration in motor unit behavior is likely maladaptive. Whereas an increase in the number of active diaphragm motor units is beneficial to muscle contraction, the overall magnitude of diaphragm EMG activity in *mdx* mice was significantly decreased. This suggests that small motor units dominate the composite EMG recording in *mdx* mice, which in turn signifies the loss of large motor units (and failure to recruit large motor units during chemostimulation). This interpretation is consistent with the loss of large myofibres in *mdx* diaphragm. Collectively, we conclude that neuromuscular control of the diaphragm is impaired in dystrophic disease, with changes presenting as early as 8 weeks in the *mdx* mouse.

Despite neuromuscular structural remodelling, profound muscle weakness, and lower EMG activity in *mdx* diaphragm, inspiratory pressure-generating capacity is remarkably preserved across ventilatory (chemoactivated breathing and augmented breaths) and non-ventilatory behaviours (sustained tracheal occlusion) (Burns *et al.*, 2019c), revealing a role for accessory and auxiliary muscles in support of peak inspiratory pressure generation in dystrophic disease (Burns *et al.*, 2019b). Interestingly, a recent study by Barnard *et al.*, (2019) assessed respiratory muscle quality and function in DMD using magnetic resonance imaging (MRI) and their findings were surprising (Barnard *et al.*, 2019). They demonstrated signs of minimal visible fatty infiltration in the intercostal muscles of DMD patients. This is one of the first cases whereby intercostal muscle sparing has been reported in DMD.

With respect to the external intercostals in this study, there was no observed difference between WT and *mdx* animals in terms of EMG activity and motor unit properties. At baseline, the EMG amplitude, number of active motor units and instantaneous firing frequencies of these units were equivalent in WT and *mdx*. Further to this, upon chemostimulation, the EMG activity was also similar comparing the two genotypes. The lack of difference between WT and *mdx* suggests that there may be a greater reliance on the external intercostals for breathing given that diaphragm EMG (and force) is impaired. However, of note, Burns *et al.* (2019) showed that maximum external intercostal activity during airway obstruction is reduced in

mdx compared with WT suggesting that compensatory activity in *mdx* that preserves peak inspiratory pressure generating capacity is not facilitated by the external intercostal muscles, suggesting a role for other auxiliary muscles such as the scalenes, sternocleidomastoids and trapezius muscles.

This study has also shown that EMG activity of the GG is equivalent in control and *mdx* animals, yet the number of active units is different, but instantaneous firing frequencies of units were equivalent. This suggests that central drive to the GG is normal in *mdx*, but motor unit morphometry is changed, similar to diaphragm and probably a consequence of reinnervation of damaged muscle. In response to chemostimulation, the GG EMG response was equivalent between control and *mdx* animals suggesting a functioning capacity for *mdx* to preserve neural control of the upper airway at least in early disease. Despite preserved EMG response to chemo-challenge in *mdx* mice, upper airway muscle weakness has been previously demonstrated in *mdx* (Burns 2016, Attal 2000), which may have implications for the maintenance of airway patency. It would be interesting to determine if GG EMG activity in response to upper airway occlusion is altered in *mdx* mice, which would suggest increased vulnerability to airway collapse, a substrate for the development of OSA.

This thesis examined breathing, respiratory muscle EMG activity and respiratory muscle motor unit behavior in the *mdx* mouse model of DMD. In conclusion, the severe mechanical disadvantage of the diaphragm is evident across a range of stimulations, yet there is a preserved capacity to raise ventilation in young *mdx* mice. Motor unit remodeling is evident in the diaphragm of *mdx* mice, but ultimately diaphragm EMG activity is impaired. The combination of reduced neural activation of the diaphragm and intrinsic weakness reveals major compromise in the neuromuscular function of the diaphragm in *mdx* mice, early in disease progression. In contrast, external intercostal motor units and EMG are relatively spared at this age across the ventilatory range, although reduced EMG activity has been observed at this early stage of dystrophic disease in response to maximum activation (Burns et al., 2019). The novel observations in this thesis coupled with other work by our group

(Burns *et al.*, 2019c) suggest that contributions from accessory muscles is critical to the support of respiratory performance in *mdx* mice, which may have relevance to DMD.

5. References

- Allen DG & Whitehead NP. (2011). Duchenne muscular dystrophy - what causes the increased membrane permeability in skeletal muscle? *Int J Biochem Cell Biol* **43**, 290-294.
- Ambrósio CE, Fadel L, Gaiad TP, Martins DS, Araújo KP, Zucconi E, Brolio MP, Giglio RF, Morini AC, Jazedje T, Froes TR, Feitosa ML, Valadares MC, Beltrão-Braga PC, Meirelles FV & Miglino MA. (2009). Identification of three distinguishable phenotypes in golden retriever muscular dystrophy. *Genet Mol Res* **8**, 389-396.
- Aminoff MJ & Sears TA. (1971). Spinal integration of segmental, cortical and breathing inputs to thoracic respiratory motoneurons. *J Physiol* **215**, 557-575.
- Arechavala-Gomez V, Kinali M, Feng L, Guglieri M, Edge G, Main M, Hunt D, Lehovskiy J, Straub V, Bushby K, Sewry CA, Morgan JE & Muntoni F. (2010). Revertant fibres and dystrophin traces in Duchenne muscular dystrophy: implication for clinical trials. *Neuromuscul Disord* **20**, 295-301.
- Attal P, Coirault C, Chemla D, Blanc FX, Rocher P, Pourny JC, Bobin S & Lecarpentier Y. (2000a). Isotonic mechanics of a pharyngeal dilator muscle and diaphragm in the rat before and after fatigue. *Eur Respir J* **15**, 308-313.
- Attal P, Lambert F, Marchand-Adam S, Bobin S, Pourny JC, Chemla D, Lecarpentier Y & Coirault C. (2000b). Severe mechanical dysfunction in pharyngeal muscle from adult mdx mice. *Am J Respir Crit Care Med* **162**, 278-281.
- Barbé F, Quera-Salva MA, McCann C, Gajdos P, Raphael JC, de Lattre J & Agustí AG. (1994). Sleep-related respiratory disturbances in patients with Duchenne muscular dystrophy. *Eur Respir J* **7**, 1403-1408.
- Barnard AM, Lott DJ, Batra A, Triplett WT, Forbes SC, Riehl SL, Willcocks RJ, Smith BK, Vandenborne K & Walter GA. (2019). Imaging respiratory muscle quality and function in Duchenne muscular dystrophy. *J Neurol* **266**, 2752-2763.
- Barohn RJ, Amato AA & Griggs RC. (1998). Overview of distal myopathies: from the clinical to the molecular. *Neuromuscul Disord* **8**, 309-316.
- Barros Maranhão J, de Oliveira Moreira D, Maurício AF, de Carvalho SC, Ferretti R, Pereira JA, Santo Neto H & Marques MJ. (2015). Changes in caldesmon, TNF- α , TGF- β and MyoD levels during the progression of skeletal muscle dystrophy in mdx mice: a comparative analysis of the quadriceps, diaphragm and intrinsic laryngeal muscles. *Int J Exp Pathol* **96**, 285-293.
- Beck J, Weinberg J, Hamnegård CH, Spahija J, Olofson J, Grimby G & Sinderby C. (2006). Diaphragmatic function in advanced Duchenne muscular dystrophy. *Neuromuscul Disord* **16**, 161-167.
- Boyd JH, Petrof BJ, Hamid Q, Fraser R & Kimoff RJ. (2004). Upper airway muscle inflammation and denervation changes in obstructive sleep apnea. *Am J Respir Crit Care Med* **170**, 541-546.

- Bradford A, McGuire M & O'Halloran KD. (2005). Does episodic hypoxia affect upper airway dilator muscle function? Implications for the pathophysiology of obstructive sleep apnoea. *Respir Physiol Neurobiol* **147**, 223-234.
- Brouns I, Pintelon I, Timmermans JP & Adriaensen D. (2012). Novel insights in the neurochemistry and function of pulmonary sensory receptors. *Adv Anat Embryol Cell Biol* **211**, 1-115, vii.
- Bulfield G, Siller WG, Wight PA & Moore KJ. (1984). X chromosome-linked muscular dystrophy (mdx) in the mouse. *Proc Natl Acad Sci U S A* **81**, 1189-1192.
- Burns DP, Canavan L, Rowland J, O'Flaherty R, Brannock M, Drummond SE, O'Malley D, Edge D & O'Halloran KD. (2018). Recovery of respiratory function in mdx mice co-treated with neutralizing interleukin-6 receptor antibodies and urocortin-2. *J Physiol*. 2018 Nov;596(21):5175-5197
- Burns DP, Drummond SE, Bolger D, Coiscaud A, Murphy KH, Edge D & O'Halloran KD. (2019a). N-acetylcysteine Decreases Fibrosis and Increases Force-Generating Capacity of *mdx* Diaphragm. *Antioxidants (Basel)* **8**. (12):581
- Burns DP, Edge D, O'Malley D & O'Halloran KD. (2015). Respiratory Control in the mdx Mouse Model of Duchenne Muscular Dystrophy. *Adv Exp Med Biol* **860**, 239-244.
- Burns DP, Lucking EF & O'Halloran KD. (2019b). Reply from David P. Burns, Eric F. Lucking and Ken D. O'Halloran: Auxiliary compensation for diaphragm dysfunction in dystrophic disease. *J Physiol* **597**, 4103-4105.
- Burns DP, Murphy KH, Lucking EF & O'Halloran KD. (2019c). Inspiratory pressure-generating capacity is preserved during ventilatory and non-ventilatory behaviours in young dystrophic mdx mice despite profound diaphragm muscle weakness. *J Physiol* **597**, 831-848.
- Burns DP & O'Halloran KD. (2016). Evidence of hypoxic tolerance in weak upper airway muscle from young mdx mice. *Respir Physiol Neurobiol* **226**, 68-75.
- Burns DP, Rowland J, Canavan L, Murphy KH, Brannock M, O'Malley D, O'Halloran KD & Edge D. (2017a). Restoration of pharyngeal dilator muscle force in dystrophin-deficient (mdx) mice following co-treatment with neutralizing interleukin-6 receptor antibodies and urocortin 2. *Exp Physiol* **102**, 1177-1193.
- Burns DP, Roy A, Lucking EF, McDonald FB, Gray S, Wilson RJ, Edge D & O'Halloran KD. (2017b). Sensorimotor control of breathing in the mdx mouse model of Duchenne muscular dystrophy. *J Physiol* **595**, 6653-6672.
- Chaudhari MR, Fallavollita JA & Farkas GA. (2016). The effects of experimental sleep apnea on cardiac and respiratory functions in 6 and 18 month old dystrophic (mdx) mice. *PLoS One* **11**, e0147640.

- Chung J, Smith AL, Hughes SC, Niizawa G, Abdel-Hamid HZ, Naylor EW, Hughes T & Clemens PR. (2016). Twenty-year follow-up of newborn screening for patients with muscular dystrophy. *Muscle Nerve* **53**, 570-578.
- Cirak S, Arechavala-Gomez V, Guglieri M, Feng L, Torelli S, Anthony K, Abbs S, Garralda ME, Bourke J, Wells DJ, Dickson G, Wood MJ, Wilton SD, Straub V, Kole R, Shrewsbury SB, Sewry C, Morgan JE, Bushby K & Muntoni F. (2011). Exon skipping and dystrophin restoration in patients with Duchenne muscular dystrophy after systemic phosphorodiamidate morpholino oligomer treatment: an open-label, phase 2, dose-escalation study. *Lancet* **378**, 595-605.
- Coirault C, Lambert F, Marchand-Adam S, Attal P, Chemla D & Lecarpentier Y. (1999). Myosin molecular motor dysfunction in dystrophic mouse diaphragm. *Am J Physiol* **277**, C1170-1176.
- Coirault C, Pignol B, Cooper RN, Butler-Browne G, Chabrier PE & Lecarpentier Y. (2003). Severe muscle dysfunction precedes collagen tissue proliferation in mdx mouse diaphragm. *J Appl Physiol* (1985) **94**, 1744-1750.
- Cros D, Harnden P, Pellissier JF & Serratrice G. (1989). Muscle hypertrophy in Duchenne muscular dystrophy. A pathological and morphometric study. *J Neurol* **236**, 43-47.
- Dale-Nagle EA, Hoffman MS, MacFarlane PM, Satriotomo I, Lovett-Barr MR, Vinit S & Mitchell GS. (2010). Spinal plasticity following intermittent hypoxia: implications for spinal injury. *Ann N Y Acad Sci* **1198**, 252-259.
- Dangain J & Vrbova G. (1984). Muscle development in mdx mutant mice. *Muscle Nerve* **7**, 700-704.
- De Bruin PF, Ueki J, Bush A, Khan Y, Watson A & Pride NB. (1997). Diaphragm thickness and inspiratory strength in patients with Duchenne muscular dystrophy. *Thorax* **52**, 472-475.
- Deconinck N & Dan B. (2007). Pathophysiology of Duchenne muscular dystrophy: current hypotheses. *Pediatr Neurol* **36**, 1-7.
- Drachman DB, Toyka KV & Myer E. (1974). Prednisone in Duchenne muscular dystrophy. *Lancet* **2**, 1409-1412.
- Eckert DJ & Malhotra A. (2008). Pathophysiology of adult obstructive sleep apnea. *Proc Am Thorac Soc* **5**, 144-153.
- Emery AE. (1991). Population frequencies of inherited neuromuscular diseases - a world survey. *Neuromuscul Disord* **1**, 19-29.
- Ervasti JM & Campbell KP. (1991). Membrane organization of the dystrophin-glycoprotein complex. *Cell* **66**, 1121-1131.
- Fallat RJ, Jewitt B, Bass M, Kamm B & Norris FH. (1979). Spirometry in amyotrophic lateral sclerosis. *Arch Neurol* **36**, 74-80.

- Falzarano MS, Passarelli C & Ferlini A. (2014). Nanoparticle delivery of antisense oligonucleotides and their application in the exon skipping strategy for Duchenne muscular dystrophy. *Nucleic Acid Ther* **24**, 87-100.
- Falzarano MS, Scotton C, Passarelli C & Ferlini A. (2015). Duchenne Muscular Dystrophy: From Diagnosis to Therapy. *Molecules* **20**, 18168-18184.
- Feldman JL, Del Negro CA & Gray PA. (2013). Understanding the rhythm of breathing: so near, yet so far. *Annu Rev Physiol* **75**, 423-452.
- Feldman JL, Mitchell GS & Nattie EE. (2003). Breathing: rhythmicity, plasticity, chemosensitivity. *Annu Rev Neurosci* **26**, 239-266.
- Fong PY, Turner PR, Denetclaw WF & Steinhardt RA. (1990). Increased activity of calcium leak channels in myotubes of Duchenne human and mdx mouse origin. *Science* **250**, 673-676.
- Fregosi RF & Mitchell GS. (1994). Long-term facilitation of inspiratory intercostal nerve activity following carotid sinus nerve stimulation in cats. *J Physiol* **477 (Pt 3)**, 469-479.
- Fukada S, Morikawa D, Yamamoto Y, Yoshida T, Sumie N, Yamaguchi M, Ito T, Miyagoe-Suzuki Y, Takeda S, Tsujikawa K & Yamamoto H. (2010). Genetic background affects properties of satellite cells and mdx phenotypes. *Am J Pathol* **176**, 2414-2424.
- Gayraud J, Matecki S, Hnia K, Mornet D, Prefaut C, Mercier J, Michel A & Ramonatxo M. (2007). Ventilation during air breathing and in response to hypercapnia in 5 and 16 month-old mdx and C57 mice. *J Muscle Res Cell Motil* **28**, 29-37.
- Golder FJ, Fuller DD, Lovett-Barr MR, Vinit S, Resnick DK & Mitchell GS. (2011). Breathing patterns after mid-cervical spinal contusion in rats. *Exp Neurol* **231**, 97-103.
- Gonzalez-Rothi EJ, Lee KZ, Dale EA, Reier PJ, Mitchell GS & Fuller DD. (2015). Intermittent hypoxia and neurorehabilitation. *J Appl Physiol* **119**, 1455-1465.
- Goshgarian HG. (2003). The crossed phrenic phenomenon: a model for plasticity in the respiratory pathways following spinal cord injury. *J Appl Physiol* **94**, 795-810.
- Gosselin LE, Barkley JE, Spencer MJ, McCormick KM & Farkas GA. (2003). Ventilatory dysfunction in mdx mice: impact of tumor necrosis factor-alpha deletion. *Muscle Nerve* **28**, 336-343.
- Gosselin LE & Williams JE. (2006). Pentoxifylline fails to attenuate fibrosis in dystrophic (mdx) diaphragm muscle. *Muscle Nerve* **33**, 820-823.
- Goyenvallé A, Vulin A, Fougère F, Leturcq F, Kaplan JC, Garcia L & Danos O. (2004). Rescue of dystrophic muscle through U7 snRNA-mediated exon skipping. *Science* **306**, 1796-1799.
- Gransee HM, Mantilla CB & Sieck GC. (2012). Respiratory muscle plasticity. *Compr Physiol* **2**, 1441-1462.

- Grounds MD, Radley HG, Lynch GS, Nagaraju K & De Luca A. (2008). Towards developing standard operating procedures for pre-clinical testing in the mdx mouse model of Duchenne muscular dystrophy. *Neurobiol Dis* **31**, 1-19.
- Grundy D. (2015). Principles and standards for reporting animal experiments in The Journal of Physiology and Experimental Physiology. *J Physiol* **593**, 2547-2549.
- Guiraud S, Squire SE, Edwards B, Chen H, Burns DT, Shah N, Babbs A, Davies SG, Wynne GM, Russell AJ, Elsey D, Wilson FX, Tinsley JM & Davies KE. (2015). Second-generation compound for the modulation of utrophin in the therapy of DMD. *Hum Mol Genet* **24**, 4212-4224.
- Gumerson JD & Michele DE. (2011). The dystrophin-glycoprotein complex in the prevention of muscle damage. *J Biomed Biotechnol* **2011**, 210797.
- Gutpell KM, Hrinivich WT & Hoffman LM. (2015). Skeletal muscle fibrosis in the mdx/utrn^{+/-} mouse validates its suitability as a murine model of Duchenne muscular dystrophy. *PLoS One* **10**, e0117306.
- Hall JE. (2011). *Guyton and Hall Textbook of Medical Physiology*. Elsevier.
- Henneman E, Somjen G & Capenter DO. (1965). Functional significance of cell size in spinal motoneurons. *J Neurophysiol* **28**, 560-580.
- Hill NS, Redline S, Carskadon MA, Curran FJ & Millman RP. (1992). Sleep-disordered breathing in patients with Duchenne muscular dystrophy using negative pressure ventilators. *Chest* **102**, 1656-1662.
- Hoen PA, van der Wees CG, Aartsma-Rus A, Turk R, Goyenvallé A, Danos O, Garcia L, van Ommen GJ, den Dunnen JT & van Deutekom JC. (2006). Gene expression profiling to monitor therapeutic and adverse effects of antisense therapies for Duchenne muscular dystrophy. *Pharmacogenomics* **7**, 281-297.
- Hoffman EP, Brown RH & Kunkel LM. (1987). Dystrophin: the protein product of the Duchenne muscular dystrophy locus. *Cell* **51**, 919-928.
- Huang P, Cheng G, Lu H, Aronica M, Ransohoff RM & Zhou L. (2011). Impaired respiratory function in mdx and mdx/utrn^(+/-) mice. *Muscle Nerve* **43**, 263-267.
- Huang P, Zhao XS, Fields M, Ransohoff RM & Zhou L. (2009). Imatinib attenuates skeletal muscle dystrophy in mdx mice. *FASEB J* **23**, 2539-2548.
- Ishizaki M, Suga T, Kimura E, Shiota T, Kawano R, Uchida Y, Uchino K, Yamashita S, Maeda Y & Uchino M. (2008). Mdx respiratory impairment following fibrosis of the diaphragm. *Neuromuscul Disord* **18**, 342-348.
- Johnson RA & Mitchell GS. (2013). Common mechanisms of compensatory respiratory plasticity in spinal neurological disorders. *Respir Physiol Neurobiol* **189**, 419-428.
- Johnson SM & Mitchell GS. (2002). Activity-dependent plasticity in descending synaptic inputs to respiratory spinal motoneurons. *Respir Physiol Neurobiol* **131**, 79-90.

- Khan Y & Heckmatt JZ. (1994). Obstructive apnoeas in Duchenne muscular dystrophy. *Thorax* **49**, 157-161.
- Khirani S, Ramirez A, Aubertin G, Boulé M, Chemouny C, Forin V & Fauroux B. (2014). Respiratory muscle decline in Duchenne muscular dystrophy. *Pediatr Pulmonol* **49**, 473-481.
- Kirk VG, Flemons WW, Adams C, Rimmer KP & Montgomery MD. (2000). Sleep-disordered breathing in Duchenne muscular dystrophy: a preliminary study of the role of portable monitoring. *Pediatr Pulmonol* **29**, 135-140.
- Koeppen BM & Stanton BA. (2010). *Berne and Levy Physiology*. Elsevier.
- Krakora D, Macrander C & Suzuki M. (2012). Neuromuscular junction protection for the potential treatment of amyotrophic lateral sclerosis. *Neurol Res Int* **2012**, 379657.
- Krieger J, Sforza E, Apprill M, Lampert E, Weitzenblum E & Ratomaharo J. (1989). Pulmonary hypertension, hypoxemia, and hypercapnia in obstructive sleep apnea patients. *Chest* **96**, 729-737.
- Kumar P & Prabhakar NR. (2012). Peripheral chemoreceptors: function and plasticity of the carotid body. *Compr Physiol* **2**, 141-219.
- Kuna ST & Vanoye CR. (1997). Respiratory-related pharyngeal constrictor muscle activity in decerebrate cats. *J Appl Physiol* **83**, 1588-1594.
- Labanowski M, Schmidt-Nowara W & Guilleminault C. (1996). Sleep and neuromuscular disease: frequency of sleep-disordered breathing in a neuromuscular disease clinic population. *Neurology* **47**, 1173-1180.
- Lane MA, Lee KZ, Salazar K, O'Steen BE, Bloom DC, Fuller DD & Reier PJ. (2012). Respiratory function following bilateral mid-cervical contusion injury in the adult rat. *Exp Neurol* **235**, 197-210.
- Redox remodeling is pivotal in murine diaphragm muscle adaptation to chronic sustained hypoxia. *Am J Respir Cell Mol Biol* **55**, 12-23.
- Lewis P, Sheehan D, Soares R, Varela Coelho A & O'Halloran KD. (2015). Chronic sustained hypoxia-induced redox remodeling causes contractile dysfunction in mouse sternohyoid muscle. *Front Physiol* **6**, 122.
- Lidov HG. (1996). Dystrophin in the nervous system. *Brain Pathol* **6**, 63-77.
- Lieber RL. (2002). *Skeletal Muscle Structure, Function & Plasticity*. Lippincott Williams & Wilkins.
- LoMauro A, D'Angelo MG & Aliverti A. (2017). Sleep Disordered Breathing in Duchenne Muscular Dystrophy. *Curr Neurol Neurosci Rep* **17**, 44.
- Lovett-Barr MR, Satriotomo I, Muir GD, Wilkerson JE, Hoffman MS, Vinit S & Mitchell GS. (2012). Repetitive intermittent hypoxia induces respiratory and somatic motor recovery after chronic cervical spinal injury. *J Neurosci* **32**, 3591-3600.

- Lu QL, Rabinowitz A, Chen YC, Yokota T, Yin H, Alter J, Jadoon A, Bou-Gharios G & Partridge T. (2005). Systemic delivery of antisense oligoribonucleotide restores dystrophin expression in body-wide skeletal muscles. *Proc Natl Acad Sci U S A* **102**, 198-203.
- Lyall RA, Donaldson N, Polkey MI, Leigh PN & Moxham J. (2001). Respiratory muscle strength and ventilatory failure in amyotrophic lateral sclerosis. *Brain* **124**, 2000-2013.
- Mantilla CB, Seven YB & Sieck GC. (2014). Convergence of pattern generator outputs on a common mechanism of diaphragm motor unit recruitment. *Prog Brain Res* **209**, 309-329.
- Mantilla CB & Sieck GC. (2003). Invited review: Mechanisms underlying motor unit plasticity in the respiratory system. *J Appl Physiol (1985)* **94**, 1230-1241.
- Mantilla CB & Sieck GC. (2011). Phrenic motor unit recruitment during ventilatory and non-ventilatory behaviors. *Respir Physiol Neurobiol* **179**, 57-63.
- Marques MJ, Oggiam DS, Barbin IC, Ferretti R & Santo Neto H. (2009). Long-term therapy with deflazacort decreases myocardial fibrosis in mdx mice. *Muscle Nerve* **40**, 466-468.
- Maskrey M, Evans SE, Mesch U, Andersen NA & Sherrey JH. (1992). Phrenicotomy in the rat: acute changes in blood gases, pH and body temperature. *Respir Physiol* **90**, 47-54.
- Mathew OP. (1984). Upper airway negative-pressure effects on respiratory activity of upper airway muscles. *J Appl Physiol Respir Environ Exerc Physiol* **56**, 500-505.
- Mayer OH, Finkel RS, Rummey C, Benton MJ, Glanzman AM, Flickinger J, Lindström BM & Meier T. (2015). Characterization of pulmonary function in Duchenne Muscular Dystrophy. *Pediatr Pulmonol* **50**, 487-494.
- Mayeux V, Corcia P, Besson G, Jafari-Schluep HF, Briolotti V & Camu W. (2003). N19S, a new SOD1 mutation in sporadic amyotrophic lateral sclerosis: no evidence for disease causation. *Ann Neurol* **53**, 815-818.
- McClore G, Moulton HM, Iversen PL, Fletcher S & Wilton SD. (2006). Antisense oligonucleotide-induced exon skipping restores dystrophin expression in vitro in a canine model of DMD. *Gene Ther* **13**, 1373-1381.
- McMahon TA. (1984). *Muscles, reflexes, and locomotion*. Princeton University Press, Princeton, N.J.; Guildford.
- Meier T, Rummey C, Leinonen M, Spagnolo P, Mayer OH, Buyse GM & Group DS. (2017). Characterization of pulmonary function in 10-18 year old patients with Duchenne muscular dystrophy. *Neuromuscul Disord* **27**, 307-314.
- Mitchell GS & Johnson SM. (2003). Neuroplasticity in respiratory motor control. *J Appl Physiol* **94**, 358-374.

- Moraes LH, de Burgos RR, Macedo AB, de Almeida Hermes T, de Faria FM & Minatel E. (2015). Reduction of Oxidative Damage and Inflammatory Response in the Diaphragm Muscle of mdx Mice Using Iron Chelator Deferoxamine. *Biol Trace Elem Res* **167**, 115-120.
- Mosqueira M, Baby SM, Lahiri S & Khurana TS. (2013). Ventilatory chemosensory drive is blunted in the mdx mouse model of Duchenne Muscular Dystrophy (DMD). *PLoS One* **8**, e69567.
- Muntoni F, Torelli S & Ferlini A. (2003). Dystrophin and mutations: one gene, several proteins, multiple phenotypes. *Lancet Neurol* **2**, 731-740.
- Nakamura A. (2015). X-Linked Dilated Cardiomyopathy: A Cardiospecific Phenotype of Dystrophinopathy. *Pharmaceuticals (Basel)* **8**, 303-320.
- Nicaise C, Hala TJ, Frank DM, Parker JL, Authelet M, Leroy K, Brion JP, Wright MC & Lepore AC. (2012). Phrenic motor neuron degeneration compromises phrenic axonal circuitry and diaphragm activity in a unilateral cervical contusion model of spinal cord injury. *Exp Neurol* **235**, 539-552.
- Nichols NL, Satriotomo I, Harrigan DJ & Mitchell GS. (2015). Acute intermittent hypoxia induced phrenic long-term facilitation despite increased SOD1 expression in a rat model of ALS. *Exp Neurol* **273**, 138-150.
- Nichols NL, Van Dyke J, Nashold L, Satriotomo I, Suzuki M & Mitchell GS. (2013). Ventilatory control in ALS. *Respir Physiol Neurobiol* **189**, 429-437.
- O'Halloran KD & Burns DP. (2018). Breathing with neuromuscular disease: Does compensatory plasticity in the motor drive to breathe offer a potential therapeutic target in muscular dystrophy? *Respir Physiol Neurobiol*. 2018.06.009
- Ogura Y, Tajrish MM, Sato S, Hindi SM & Kumar A. (2014). Therapeutic potential of matrix metalloproteinases in Duchenne muscular dystrophy. *Front Cell Dev Biol* **2**, 11.
- Ozawa E, Hagiwara Y & Yoshida M. (1999). Creatine kinase, cell membrane and Duchenne muscular dystrophy. *Mol Cell Biochem* **190**, 143-151.
- Pane M, Scalise R, Berardinelli A, D'Angelo G, Ricotti V, Alfieri P, Moroni I, Hartley L, Pera MC, Baranello G, Catteruccia M, Casalino T, Romeo DM, Graziano A, Gandioli C, Bianco F, Mazzone ES, Lombardo ME, Scoto M, Sivo S, Palermo C, Gualandi F, Sormani MP, Ferlini A, Bertini E, Muntoni F & Mercuri E. (2013). Early neurodevelopmental assessment in Duchenne muscular dystrophy. *Neuromuscul Disord* **23**, 451-455.
- Parent A. (2005). Duchenne De Boulogne: a pioneer in neurology and medical photography. *Can J Neurol Sci* **32**, 369-377.
- Petrillo S, Pelosi L, Piemonte F, Travaglini L, Forcina L, Catteruccia M, Petrini S, Verardo M, D'Amico A, Musarò A & Bertini E. (2017). Oxidative stress in Duchenne muscular dystrophy: focus on the NRF2 redox pathway. *Hum Mol Genet* **26**, 2781-2790.

- Petrof BJ, Shrager JB, Stedman HH, Kelly AM & Sweeney HL. (1993). Dystrophin protects the sarcolemma from stresses developed during muscle contraction. *Proc Natl Acad Sci U S A* **90**, 3710-3714.
- Plowman SA. (2017). *Exercise physiology for health fitness and performance*. Lippincott Williams & Wilkins.
- Polla B, D'Antona G, Bottinelli R & Reggiani C. (2004). Respiratory muscle fibres: specialisation and plasticity. *Thorax* **59**, 808-817.
- Pratt SJ, Valencia AP, Le GK, Shah SB & Lovering RM. (2015). Pre- and postsynaptic changes in the neuromuscular junction in dystrophic mice. *Front Physiol* **6**, 252.
- Reid MB. (2001). Invited Review: redox modulation of skeletal muscle contraction: what we know and what we don't. *J Appl Physiol* **90**, 724-731.
- Remmers JE, deGroot WJ, Sauerland EK & Anch AM. (1978). Pathogenesis of upper airway occlusion during sleep. *J Appl Physiol Respir Environ Exerc Physiol* **44**, 931-938.
- Rice A, Fuglevand AJ, Laine CM & Fregosi RF. (2011). Synchronization of presynaptic input to motor units of tongue, inspiratory intercostal, and diaphragm muscles. *J Neurophysiol* **105**, 2330-2336.
- Roberts JL, Reed WR & Thach BT. (1984). Pharyngeal airway-stabilizing function of sternohyoid and sternothyroid muscles in the rabbit. *J Appl Physiol* **57**, 1790-1795.
- Rodrigues M, Echigoya Y, Fukada SI & Yokota T. (2016). Current Translational Research and Murine Models For Duchenne Muscular Dystrophy. *J Neuromuscul Dis* **3**, 29-48.
- Sali A, Guerron AD, Gordish-Dressman H, Spurney CF, Iantorno M, Hoffman EP & Nagaraju K. (2012). Glucocorticoid-treated mice are an inappropriate positive control for long-term preclinical studies in the mdx mouse. *PLoS One* **7**, e34204.
- Sauerland EK & Harper RM. (1976). The human tongue during sleep: electromyographic activity of the genioglossus muscle. *Exp Neurol* **51**, 160-170.
- Schara U, Mortier & Mortier W. (2001). Long-Term Steroid Therapy in Duchenne Muscular Dystrophy-Positive Results versus Side Effects. *J Clin Neuromuscul Dis* **2**, 179-183.
- Scheuerbrandt G, Lundin A, Lövgren T & Mortier W. (1986). Screening for Duchenne muscular dystrophy: an improved screening test for creatine kinase and its application in an infant screening program. *Muscle Nerve* **9**, 11-23.
- Schiaffino S & Reggiani C. (2011). Fiber types in mammalian skeletal muscles. *Physiol Rev* **91**, 1447-1531.
- Seven YB, Nichols NL, Kelly MN, Hobson OR, Satriotomo I & Mitchell GS. (2018). Compensatory plasticity in diaphragm and intercostal muscle utilization in a rat model of ALS. *Exp Neurol* **299**, 148-156.

- Sherrey JH, Pollard MJ & Megirian D. (1986). Respiratory functions of the inferior pharyngeal constrictor and sternohyoid muscles during sleep. *Exp Neurol* **92**, 267-277.
- Sherrington CS. (1935). Sir Edward Sharpey-Schafer and His Contributions to Neurology. *Edinb Med J* **42**, 393-406.
- Sieck GC, Ferreira LF, Reid MB & Mantilla CB. (2013). Mechanical properties of respiratory muscles. *Compr Physiol* **3**, 1553-1567.
- Sieck GC & Fournier M. (1989). Diaphragm motor unit recruitment during ventilatory and nonventilatory behaviors. *J Appl Physiol* **66**, 2539-2545.
- Smith PE, Edwards RH & Calverley PM. (1989a). Oxygen treatment of sleep hypoxaemia in Duchenne muscular dystrophy. *Thorax* **44**, 997-1001.
- Smith PE, Edwards RH & Calverley PM. (1989b). Ventilation and breathing pattern during sleep in Duchenne muscular dystrophy. *Chest* **96**, 1346-1351.
- Stedman HH, Sweeney HL, Shrager JB, Maguire HC, Panettieri RA, Petrof B, Narusawa M, Leferovich JM, Sladky JT & Kelly AM. (1991). The mdx mouse diaphragm reproduces the degenerative changes of Duchenne muscular dystrophy. *Nature* **352**, 536-539.
- Stewart H, Eisen A, Road J, Mezei M & Weber M. (2001). Electromyography of respiratory muscles in amyotrophic lateral sclerosis. *J Neurol Sci* **191**, 67-73.
- Suresh S, Wales P, Dakin C, Harris MA & Cooper DG. (2005). Sleep-related breathing disorder in Duchenne muscular dystrophy: disease spectrum in the paediatric population. *J Paediatr Child Health* **41**, 500-503.
- Talakad N S, Pradhan C, Nalini A, Thennarasu K & Raju TR. (2009). Assessment of pulmonary function in amyotrophic lateral sclerosis. *Indian J Chest Dis Allied Sci* **51**, 87-91.
- Tinsley J, Robinson N & Davies KE. (2015). Safety, tolerability, and pharmacokinetics of SMT C1100, a 2-arylbenzoxazole utrophin modulator, following single- and multiple-dose administration to healthy male adult volunteers. *J Clin Pharmacol* **55**, 698-707.
- Toussaint M, Davidson Z, Bouvoie V, Evenepoel N, Haan J & Soudon P. (2016). Dysphagia in Duchenne muscular dystrophy: practical recommendations to guide management. *Disabil Rehabil* **38**, 2052-2062.
- Turner PR, Schultz R, Ganguly B & Steinhardt RA. (1993). Proteolysis results in altered leak channel kinetics and elevated free calcium in mdx muscle. *J Membr Biol* **133**, 243-251.
- Van de Graaff WB, Gottfried SB, Mitra J, van Lunteren E, Cherniack NS & Strohl KP. (1984). Respiratory function of hyoid muscles and hyoid arch. *J Appl Physiol* **57**, 197-204.

- van der Pijl EM, van Putten M, Niks EH, Verschuuren JJ, Aartsma-Rus A & Plomp JJ. (2016). Characterization of neuromuscular synapse function abnormalities in multiple Duchenne muscular dystrophy mouse models. *Eur J Neurosci* **43**, 1623-1635.
- van Lunteren E, Haxhiu MA & Cherniack NS. (1987). Relation between upper airway volume and hyoid muscle length. *J Appl Physiol* **63**, 1443-1449.
- Vinit S, Lovett-Barr MR & Mitchell GS. (2009). Intermittent hypoxia induces functional recovery following cervical spinal injury. *Respir Physiol Neurobiol* **169**, 210-217.
- Wagner MH & Berry RB. (2008). Disturbed sleep in a patient with Duchenne muscular dystrophy. *J Clin Sleep Med* **4**, 173-175.
- Wehling-Henricks M, Lee JJ & Tidball JG. (2004). Prednisolone decreases cellular adhesion molecules required for inflammatory cell infiltration in dystrophin-deficient skeletal muscle. *Neuromuscul Disord* **14**, 483-490.
- White DP. (2005). Pathogenesis of obstructive and central sleep apnea. *Am J Respir Crit Care Med* **172**, 1363-1370.
- Wiegand DA, Latz B, Zwillich CW & Wiegand L. (1990). Geniohyoid muscle activity in normal men during wakefulness and sleep. *J Appl Physiol* **69**, 1262-1269.
- Wu B, Cloer C, Lu P, Milazi S, Shaban M, Shah SN, Marston-Poe L, Moulton HM & Lu QL. (2014). Exon skipping restores dystrophin expression, but fails to prevent disease progression in later stage dystrophic dko mice. *Gene Ther* **21**, 785-793.
- Yiu EM & Kornberg AJ. (2008). Duchenne muscular dystrophy. *Neurol India* **56**, 236-247.

6. Publications

- Burns DP, Drummond SE, Bolger D, Coiscand A, Murphy KH, Edge D & O'Halloran KD "N-acetylcysteine decreases fibrosis and increases force-generating capacity of *mdx* diaphragm". *Antioxidants*, 8(12) pii: E581. [doi:10.3390/antiox8120581](https://doi.org/10.3390/antiox8120581).
- Burns DP, Murphy KH, Lucking EF & O'Halloran KD (2019) "Inspiratory pressure-generating capacity is preserved during ventilatory and non-ventilatory behaviours in young adult male dystrophic (*mdx*) mice despite profound diaphragm muscle weakness". *The Journal of Physiology*, [597\(3\):831-848](https://doi.org/10.1111/jphysiol.5973).
- Lucking EF, Murphy KH, Burns DP, Jaisimha AV, Barry-Murphy KJ, Boland B, Rae MG & O'Halloran KD (2018) "No evidence in support of a prodromal respiratory control signature in the TgF344-AD rat model of Alzheimer's disease". *Respiratory Physiology and Neurobiology*, [doi:10.1016/j.resp.2018.06.014](https://doi.org/10.1016/j.resp.2018.06.014).
- O'Halloran KD, Murphy KH & Burns DP (2017) "Antioxidant therapy for muscular dystrophy: Caveat lector!". *The Journal of Physiology*, [596\(4\):737-738](https://doi.org/10.1111/jphysiol.5964).
- Burns DP, Rowland J, Canavan L, Murphy KH, Brannock M, O'Malley D, O'Halloran KD & Edge D (2017) "Restoration of pharyngeal dilator muscle force in dystrophin deficient (*mdx*) mice following co-treatment with neutralizing IL-6 receptor antibodies and Urocortin-2". *Experimental Physiology*, [102 \(9\):1177-1193](https://doi.org/10.1111/jphysiol.1029).

7. Conference proceedings

- Experimental Biology 2018 (Orlando, USA). Burns DP, Murphy KH, Lucking EF & O'Halloran KD (2019) "Inspiratory pressure-generating capacity is preserved during ventilatory and non-ventilatory behaviours despite profound diaphragm muscle weakness in young adult dystrophic (*mdx*) mice".
- Experimental Biology 2018 (Orlando, USA). Burns DP, Drummond SE, Bolger D, Murphy KH, Coiscand A, Edge D & O'Halloran KD (2019) "N-Acetyl cysteine improves dystrophic (*mdx*) mouse diaphragm muscle quality and strength".
- New Horizons in Medical Research UCC (Cork, IRL). Burns DP, Drummond SE, Bolger D, Murphy KH, Coiscand A, Edge D & O'Halloran KD (2018) "N-Acetyl cysteine improves dystrophic (*mdx*) mouse diaphragm muscle quality and strength" (Poster).

- Europhysiology 2018 (London, UK). The Physiological Society. Burns DP, O'Driscoll E, Rowland J, Canavan L, Murphy KH, O'Connor KM, O'Malley D, Clarke G, Edge D & O'Halloran KD (2018) "Breathing with neuromuscular disease: insights from pre-clinical studies" (Selected talk).
- Experimental Biology 2018 (San Diego, USA). American Physiological Society. Murphy KH, Burns DP, Lucking EF & O'Halloran KD (2018) "Respiratory EMG responsiveness to hypercapnic hypoxia in *mdx* mice" (Poster).
- Experimental Biology 2018 (San Diego, USA). American Physiological Society. Burns DP, Edge D, Murphy KH & O'Halloran KD (2018) "Chronic intermittent hypoxia enhances respiratory muscle weakness in dystrophin-deficient *mdx* mice" (Poster).
- Oxford Control of Breathing Meeting (Oxford, UK). Murphy KH, Burns DP, Barry-Murphy K, Rae MG, O'Halloran KD & Lucking EF (2017) "Respiratory control in a rat model of Alzheimer's disease" (Poster).
- Royal Academy of Medicine in Ireland Biomedical Sciences Meeting 2017 (Dublin, IRL). Murphy KH, Burns DP, Barry-Murphy K, Rae MG, O'Halloran KD & Lucking EF (2017) "Respiratory control in a rat model of Alzheimer's disease" (Poster).
- Experimental Biology 2017 (Chicago, USA). American Physiological Society. Murphy KH, Burns DP, Barry-Murphy K, Rae M, O'Halloran KD & Lucking EF (2017) "Respiratory control in a rat model of Alzheimer's disease (TgF344-AD)" (Poster).
- New Horizons in Medical Research UCC (Cork, IRL). Murphy KH, Burns DP, Rowland J, Canavan L, O'Malley D, O'Halloran KD & Edge D (2016) "Restoration of pharyngeal dilator muscle force in dystrophin-deficient (*mdx*) mice following co-treatment with neutralizing IL-6R antibody and Urocortin-2" (Poster).
- Physiology 2016 (Dublin, IRL). Burns DP, Rowland J, Canavan L, Murphy KH, O'Malley D, O'Halloran KD & Edge D (2016) "Restoration of pharyngeal dilator muscle force in dystrophin-deficient (*mdx*) mice following co-treatment with neutralizing IL-6R antibody and Urocortin-2" (Poster).
- Royal Academy of Medicine in Ireland Biomedical Sciences Meeting 2016 (Cork, IRL). Murphy KH, Burns DP, Rowland J, Canavan L, O'Malley D, O'Halloran KD & Edge D (2016) "Restoration of pharyngeal dilator muscle force in dystrophin deficient (*mdx*) mice following co-treatment with neutralizing IL-6R antibody and urocortin-2" (Selected talk).